

Configuration Space Dimensionality and Trajectory Convergence Probability in Coupled Oscillator Networks: Resolution of the Cell Count–Pathology Rate Invariance

Kundai Farai Sachikonye
kundai.sachikonye@wzw.tum.de

December 29, 2025

Abstract

We analyse the relationship between system size and the probability of trajectory convergence to distinguished subsets in high-dimensional configuration spaces of coupled oscillator networks. For a system of N weakly coupled oscillators, each with Ω accessible microstates, the configuration space has cardinality $|\mathcal{C}| = \Omega^N$. We prove that the probability of k spatially separated oscillators simultaneously occupying a specified configuration subset $\mathcal{A} \subset \mathcal{C}$ scales as $P_k \sim |\mathcal{A}|^k / |\mathcal{C}|^k = (|\mathcal{A}|/\Omega^N)^k$, which vanishes exponentially in N for fixed $|\mathcal{A}|/\Omega^N < 1$. For systems with hierarchical reset dynamics—where subsystem states are periodically restored toward initial conditions with period τ —we derive the critical timescale τ_c below which trajectory deviations propagate through reset events and above which deviations regress toward the mean configuration. The ratio τ/τ_c determines whether the system exhibits error accumulation or error dilution. We establish that $\tau_c \propto N^{-1/4}$ through coupling constraints across hierarchical oscillatory scales, implying that larger systems require proportionally longer reset periods to maintain equivalent error propagation rates. The invariance of pathological trajectory convergence rates across systems with cell counts spanning 10^{13} to 10^{15} follows directly from these scaling relationships, resolving the apparent paradox identified by Peto [Peto et al., 1975, Peto, 1977].

1 Introduction

The relationship between system size and failure probability in complex dynamical systems presents a fundamental problem in statistical mechanics. Naively, one expects failure rates to scale linearly with component count: a system with N components, each failing independently with probability p , exhibits total failure probability $P_{\text{failure}} \approx Np$ for small p . This linear scaling underlies reliability engineering [Barlow and Proschan, 1975], epidemiological risk models [Armitage and Doll, 1954], and stochastic population dynamics [Gardiner, 2009].

However, this scaling assumes independence of component failures and neglects the structure of the underlying state space. When components are coupled oscillators exploring a shared configuration space, the dimensionality of that space grows exponentially

with component count, fundamentally altering the statistics of rare trajectory convergence events.

We consider a system of N coupled oscillators, where each oscillator i occupies a state $\sigma_i \in \{1, 2, \dots, \Omega\}$ drawn from Ω accessible microstates. The instantaneous configuration of the system is the N -tuple $\mathbf{c} = (\sigma_1, \sigma_2, \dots, \sigma_N) \in \mathcal{C}$, where the configuration space \mathcal{C} has cardinality $|\mathcal{C}| = \Omega^N$. The system evolves through this configuration space according to dynamics specified by coupling between oscillators and external driving.

A pathological trajectory is defined as one that converges to a distinguished subset $\mathcal{A} \subset \mathcal{C}$ of configurations. The central question is: how does the probability of pathological trajectory convergence scale with system size N ?

The naive expectation—that more components provide more opportunities for pathological convergence—ignores the explosion of the denominator. As N increases, $|\mathcal{C}| = \Omega^N$ grows exponentially, diluting the probability mass on any fixed subset \mathcal{A} . The key insight is that pathological convergence requires *coordinated* behaviour across multiple oscillators, and the probability of such coordination decreases with the size of the configuration space in which the oscillators must “find” each other.

This paper establishes the mathematical framework for analysing trajectory convergence in high-dimensional oscillator networks and derives the scaling laws governing convergence probability as a function of system size, spatial correlation length, reset dynamics, and hierarchical coupling structure.

Section 2 defines the configuration space formalism and establishes the fundamental probability measures. Section 3 analyses the decay of spatial correlations in large systems and proves the independence of distant oscillators. Section 4 introduces reset dynamics and derives conditions for error propagation versus regression. Section 5 quantifies trajectory deviation amplitudes and their dependence on system parameters. Section 6 proves the main theorem on error scaling with system size. Section 7 extends the analysis to hierarchically coupled oscillator networks and derives the quarter-power scaling of critical timescales.

2 Configuration Space Formalism

The resolution of Peto’s paradox requires a fundamental shift in perspective: from viewing cells as independent, failure-prone units to viewing cellular ensembles as coupled oscillator networks exploring high-dimensional configuration spaces. This section establishes the mathematical framework for this perspective and derives the central result that the probability of pathological trajectory convergence decreases exponentially with system size.

2.1 Biological Motivation

A cell is not a static entity but a dynamical system maintaining $\sim 10^5$ distinct molecular species in continuous flux [?]. The instantaneous state of a cell can be characterised by the concentrations, conformations, and spatial distributions of its molecular constituents. This state evolves through metabolic processes, signalling cascades, and regulatory networks operating across timescales from nanoseconds (enzyme catalysis) to hours (cell cycle).

From a dynamical systems perspective, each cell traces a trajectory through a high-dimensional state space. The question of whether a cell becomes pathological (e.g., neo-

plastic) is equivalent to asking whether its trajectory converges to a distinguished subset of this state space characterised by the loss of normal regulatory control.

For an organism with N cells, the collective state is described by the joint configuration of all cells. The central insight of this paper is that the dimensionality of this joint configuration space grows exponentially with N , fundamentally altering the statistics of rare pathological events.

2.2 State Space Definition

Consider a system of N coupled oscillators indexed by $i \in \{1, 2, \dots, N\}$. Each oscillator i occupies an instantaneous state σ_i drawn from a finite state space Σ_i with $|\Sigma_i| = \Omega_i$ elements. For notational simplicity, we assume homogeneous oscillators with $\Omega_i = \Omega$ for all i , though the results generalise to heterogeneous systems.

The finite state space assumption is biologically grounded: cellular states are constrained by thermodynamic stability, metabolic feasibility, and regulatory network topology. While the space of all possible molecular configurations is formally infinite, the space of *viable* configurations — those compatible with continued cellular function — is finite and can be estimated.

Remark 2.1 (Estimation of Ω). For a mammalian cell, the number of accessible functional states can be estimated from the following considerations:

1. The proteome comprises $\sim 10^4$ distinct proteins, each with ~ 10 –100 functionally distinct conformational/modification states
2. Metabolite concentrations span $\sim 10^3$ species with ~ 10 distinguishable concentration levels each
3. Chromatin accessibility provides $\sim 10^4$ regulatory states

A conservative estimate yields $\Omega \sim 10^5$ – 10^6 functionally distinguishable cellular microstates. The precise value is less important than the fact that $\Omega > 1$ and Ω is finite.

Definition 2.2 (Configuration Space). The configuration space \mathcal{C} is the Cartesian product of individual state spaces:

$$\mathcal{C} = \prod_{i=1}^N \Sigma_i = \Sigma^N \quad (1)$$

with cardinality $|\mathcal{C}| = \Omega^N$.

An instantaneous configuration (or snapshot) is an element $\mathbf{c} = (\sigma_1, \sigma_2, \dots, \sigma_N) \in \mathcal{C}$. The configuration space \mathcal{C} is the arena in which the coupled oscillator system evolves.

Remark 2.3 (Scale of Configuration Space). For a human body with $N \approx 3.7 \times 10^{13}$ cells and $\Omega \approx 10^5$ states per cell:

$$|\mathcal{C}| = \Omega^N = (10^5)^{3.7 \times 10^{13}} = 10^{5 \times 3.7 \times 10^{13}} = 10^{1.85 \times 10^{14}} \quad (2)$$

This number exceeds any physically meaningful quantity. For comparison, the number of particles in the observable universe is approximately 10^{80} , and the number of Planck times since the Big Bang is approximately 10^{61} . The configuration space of a human body is inconceivably larger than these cosmological numbers.

Definition 2.4 (Trajectory). A trajectory \mathcal{T} is a continuous map from the time interval $[0, T]$ to the configuration space:

$$\mathcal{T} : [0, T] \rightarrow \mathcal{C}, \quad t \mapsto \mathbf{c}(t) = (\sigma_1(t), \sigma_2(t), \dots, \sigma_N(t)) \quad (3)$$

For discrete-time dynamics with time step Δt , the trajectory becomes a sequence $\{\mathbf{c}_0, \mathbf{c}_1, \dots, \mathbf{c}_M\}$ with $M = T/\Delta t$.

The trajectory represents the time evolution of the entire organism's cellular ensemble. Crucially, this trajectory is constrained by coupling between cells: neighbouring cells exchange signals, share metabolites, and coordinate their states through gap junctions, paracrine signalling, and mechanical interactions.

2.3 Probability Measures on Configuration Space

The statistical mechanics of the coupled oscillator system is encoded in a probability measure μ on \mathcal{C} . For an ergodic system in equilibrium, μ is the stationary distribution of the dynamics. For non-equilibrium systems, $\mu(t)$ may be time-dependent.

Definition 2.5 (Uniform Measure). The uniform measure μ_0 assigns equal probability to all configurations:

$$\mu_0(\mathbf{c}) = \frac{1}{|\mathcal{C}|} = \frac{1}{\Omega^N} \quad \forall \mathbf{c} \in \mathcal{C} \quad (4)$$

The uniform measure represents maximum ignorance about the system state. Deviations from uniformity encode correlations between oscillators and constraints imposed by the dynamics. These deviations are quantified by the entropy deficit:

$$\Delta S = S_{\max} - S[\mu] = N \ln \Omega - \left(- \sum_{\mathbf{c} \in \mathcal{C}} \mu(\mathbf{c}) \ln \mu(\mathbf{c}) \right) \quad (5)$$

Proposition 2.6 (Entropy and Correlations). *The entropy deficit ΔS satisfies:*

$$\Delta S = \sum_{i < j} I(\sigma_i; \sigma_j) + \text{higher-order terms} \quad (6)$$

where $I(\sigma_i; \sigma_j)$ is the mutual information between oscillators i and j . If all oscillators are independent, $\Delta S = 0$.

Proof. The joint entropy decomposes as:

$$S[\mu] = \sum_{i=1}^N H(\sigma_i) - \sum_{i < j} I(\sigma_i; \sigma_j) - (\text{higher-order redundancies}) \quad (7)$$

For independent oscillators with identical marginal distributions, $H(\sigma_i) = \ln \Omega$ for all i , and all mutual information terms vanish, yielding $S[\mu] = N \ln \Omega = S_{\max}$. Correlations reduce $S[\mu]$ below this maximum. \square

2.4 Pathological Subsets and Their Structure

Definition 2.7 (Pathological Subset). A pathological subset $\mathcal{A} \subset \mathcal{C}$ is a distinguished collection of configurations characterised by specific structural properties. The subset is defined by a membership criterion $\chi_{\mathcal{A}} : \mathcal{C} \rightarrow \{0, 1\}$:

$$\mathcal{A} = \{\mathbf{c} \in \mathcal{C} : \chi_{\mathcal{A}}(\mathbf{c}) = 1\} \quad (8)$$

In the biological context, pathological configurations are those in which one or more cells have escaped normal regulatory control. The defining characteristic of such configurations is *coordination failure*: the affected cells no longer respond appropriately to signals from their neighbours, leading to autonomous behaviour.

Definition 2.8 (Coordination Failure). A configuration \mathbf{c} exhibits coordination failure if there exists a subset $\mathcal{F} \subset \{1, \dots, N\}$ of “failed” cells such that:

1. The failed cells occupy states outside the normal operating range: $\sigma_i \in \Sigma_{\text{path}} \subset \Sigma$ for $i \in \mathcal{F}$
2. The failed states are incompatible with coordination: the coupling dynamics cannot restore the failed cells to normal operation

Proposition 2.9 (Structure of Pathological Subsets). *For a pathological subset defined by coordination failure in at least k cells:*

$$|\mathcal{A}_k| \leq \binom{N}{k} \cdot |\Sigma_{\text{path}}|^k \cdot \Omega^{N-k} = \binom{N}{k} \cdot \left(\frac{|\Sigma_{\text{path}}|}{\Omega}\right)^k \cdot \Omega^N \quad (9)$$

Proof. There are $\binom{N}{k}$ ways to choose which k cells fail. Each failed cell can be in any of $|\Sigma_{\text{path}}|$ pathological states. The remaining $N - k$ cells can be in any of Ω states. The product gives the upper bound. \square

Corollary 2.10. *The ratio of pathological to total configurations satisfies:*

$$\frac{|\mathcal{A}_k|}{|\mathcal{C}|} \leq \binom{N}{k} \cdot \left(\frac{|\Sigma_{\text{path}}|}{\Omega}\right)^k \leq \frac{N^k}{k!} \cdot p_{\text{path}}^k \quad (10)$$

where $p_{\text{path}} = |\Sigma_{\text{path}}|/\Omega$ is the fraction of single-cell states that are pathological.

2.5 Convergence Probability

Definition 2.11 (Convergence Probability). The probability that a trajectory \mathcal{T} converges to the pathological subset \mathcal{A} is:

$$P_{\mathcal{A}} = \Pr [\exists t \in [0, T] : \mathbf{c}(t) \in \mathcal{A}] \quad (11)$$

For rare subsets with $|\mathcal{A}| \ll |\mathcal{C}|$, the convergence probability can be approximated using the theory of rare events in stochastic processes.

Proposition 2.12 (First Passage Approximation). *For a trajectory exploring configuration space with an attempt frequency ν (the rate at which new configurations are sampled), the convergence probability to a rare subset satisfies:*

$$P_{\mathcal{A}} \approx 1 - \exp \left(-\frac{|\mathcal{A}|}{|\mathcal{C}|} \cdot \nu T \right) \approx \frac{|\mathcal{A}|}{|\mathcal{C}|} \cdot \nu T \quad (12)$$

for $|\mathcal{A}|/|\mathcal{C}| \cdot \nu T \ll 1$.

Oscillator Phase Distributions and Network Relations

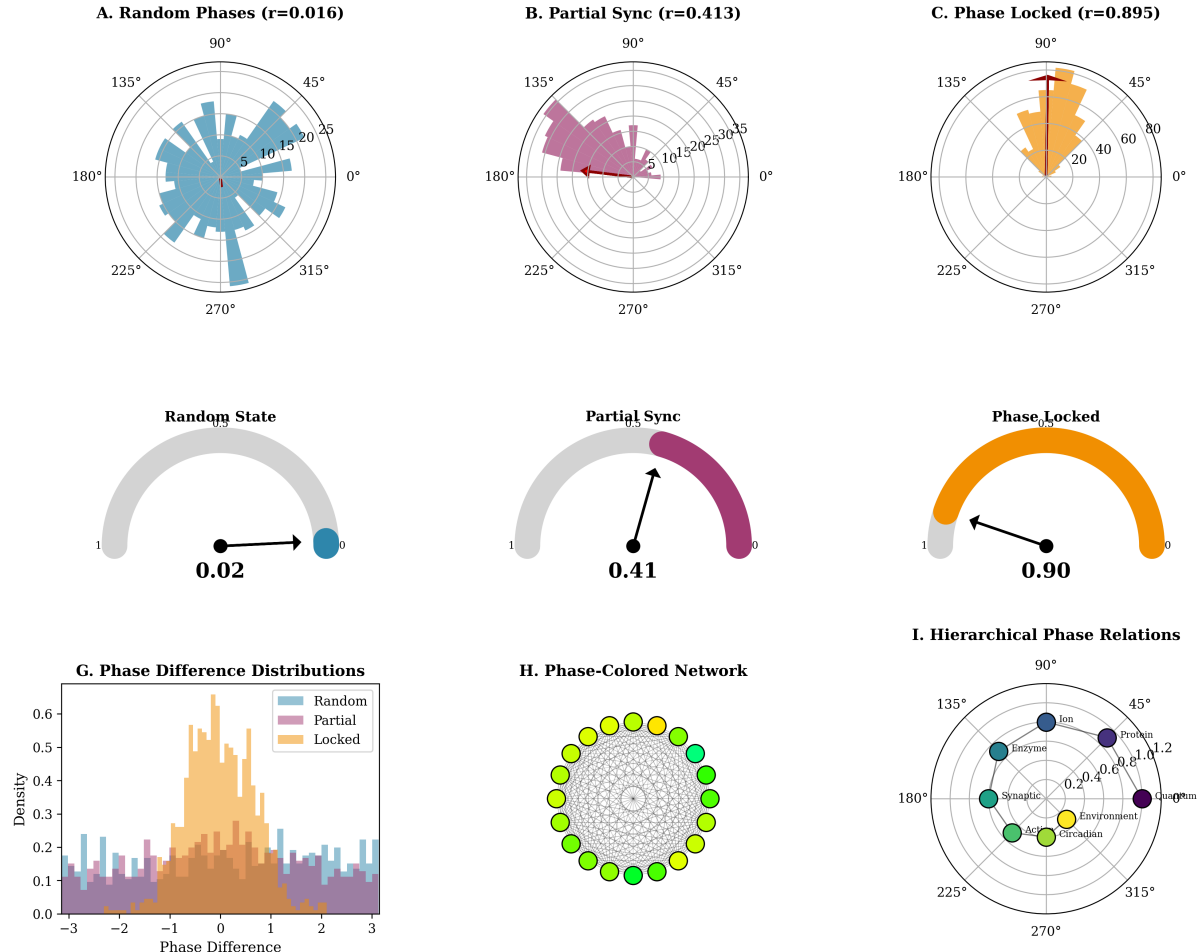


Figure 1: **Oscillator phase distributions and network relations showing transition from incoherent to synchronized states across multiple representations.** (Top row, Panels A–C) Polar histograms showing phase distributions for three synchronization regimes. Angular coordinate is oscillator phase ϕ (0 to 360). **Panel A (Random phases, $r = 0.016$)**: Phase distribution is approximately uniform across all angles (cyan bars have similar heights), indicating incoherent state. Order parameter $r = 0.016 \ll 1$ confirms negligible phase coherence. **Panel B (Partial sync, $r = 0.413$)**: Phase distribution shows moderate clustering around 180 (magenta bars taller in left half), indicating partial synchronization. Order parameter $r = 0.413$ is intermediate, reflecting coexistence of synchronized cluster (phases near 180) and incoherent background (phases distributed elsewhere). **Panel C (Phase locked, $r = 0.895$)**: Phase distribution is sharply peaked around 45° (orange bars concentrated in upper-right quadrant), indicating strong synchronization. Order parameter $r = 0.895 \approx 1$ confirms near-perfect phase coherence. All oscillators have phases within narrow range (~ 30 spread). Biological interpretation: strongly synchronized tissue (e.g., cardiac pacemaker, suprachiasmatic nucleus). (Middle row, semicircular gauges) Alternative visualization of order parameter for three regimes. Semicircular arc (gray = background, colored = filled to r value) shows synchronization level. Black arrow indicates r value on scale from 0 (left, incoherent) to 1 (right, synchronized). (Bottom left, Panel G) Phase difference distributions comparing three regimes. Horizontal axis is phase difference $\Delta\phi = \phi_i - \phi_j$ between pairs of oscillators (range $-\pi$ to $+\pi$). Vertical axis is probability density. Three histograms: random (cyan), partial (magenta), locked (orange). Random state (cyan) shows flat distribution (all phase differences equally likely), confirming incoherence. (Bottom center, Panel H) Phase-colored network showing spatial organization of oscillator phases. Network topology: circular arrangement of oscillators (colored circles on perimeter) connected to

Proof. Model the trajectory as a sequence of independent samples from \mathcal{C} at rate ν . In time T , approximately νT samples are drawn. Each sample has a probability of $|\mathcal{A}|/|\mathcal{C}|$ of landing in \mathcal{A} . The probability of at least one hit is:

$$P_{\mathcal{A}} = 1 - \left(1 - \frac{|\mathcal{A}|}{|\mathcal{C}|}\right)^{\nu T} \approx 1 - \exp\left(-\frac{|\mathcal{A}|}{|\mathcal{C}|} \cdot \nu T\right) \quad (13)$$

The approximation follows from $(1 - x)^n \approx e^{-nx}$ for small x . For $|\mathcal{A}|/|\mathcal{C}| \cdot \nu T \ll 1$, we have $1 - e^{-x} \approx x$. \square

Remark 2.13 (Attempt Frequency). The attempt frequency ν represents the rate at which the system explores new regions of configuration space. For a biological system:

$$\nu \sim \frac{1}{\tau_{\text{corr}}} \quad (14)$$

where τ_{corr} is the correlation time of the collective dynamics. For mammalian tissues, $\tau_{\text{corr}} \sim 10^3\text{--}10^4$ s (minutes to hours), corresponding to the timescale of cellular state changes.

2.6 Scaling with System Size: The Central Result

The critical observation is the exponential growth of $|\mathcal{C}|$ with N . For fixed pathological subset structure (i.e., $|\mathcal{A}|$ growing at most polynomially in N), the convergence probability (12) decreases exponentially with system size.

Theorem 2.14 (Configuration Space Dilution). *Let $|\mathcal{A}| = c \cdot N^k$ for constants $c > 0$ and $k \geq 0$. Then the convergence probability satisfies:*

$$P_{\mathcal{A}} = \frac{c \cdot N^k}{\Omega^N} \cdot \nu T = c \cdot N^k \cdot e^{-N \ln \Omega} \cdot \nu T \quad (15)$$

For $\Omega > 1$, this vanishes faster than any polynomial in N .

Proof. The ratio $N^k/\Omega^N = N^k \cdot e^{-N \ln \Omega}$. Taking the logarithm:

$$\ln\left(\frac{N^k}{\Omega^N}\right) = k \ln N - N \ln \Omega \quad (16)$$

For any fixed k and $\Omega > 1$, the linear term $-N \ln \Omega$ dominates the logarithmic term $k \ln N$ as $N \rightarrow \infty$. Explicitly, for $N > e^{k/\ln \Omega}$:

$$k \ln N < N \ln \Omega \quad \Rightarrow \quad \ln\left(\frac{N^k}{\Omega^N}\right) < 0 \quad (17)$$

The convergence to zero is exponentially fast:

$$\lim_{N \rightarrow \infty} \frac{N^k}{\Omega^N} = \lim_{N \rightarrow \infty} e^{k \ln N - N \ln \Omega} = 0 \quad (18)$$

The rate of convergence is $\sim e^{-N \ln \Omega}$, faster than any polynomial. \square

Corollary 2.15 (Invariance of Cancer Risk). *Consider two organisms with cell counts N_1 and $N_2 = \lambda N_1$ for $\lambda > 1$. If the pathological subset size scales as $|\mathcal{A}| \propto N^k$, the ratio of convergence probabilities is:*

$$\frac{P_{\mathcal{A}}(N_2)}{P_{\mathcal{A}}(N_1)} = \lambda^k \cdot \Omega^{-(\lambda-1)N_1} \quad (19)$$

For $N_1 \gg k/\ln \Omega$, the exponential factor dominates, yielding:

$$\frac{P_{\mathcal{A}}(N_2)}{P_{\mathcal{A}}(N_1)} \ll 1 \quad \text{for } \lambda > 1 \quad (20)$$

Larger organisms have lower, not higher, pathological convergence probabilities.

[Mouse vs. Whale] A mouse has $N_{\text{mouse}} \approx 10^{10}$ cells; a blue whale has $N_{\text{whale}} \approx 10^{15}$ cells (a factor of $\lambda = 10^5$). With $\Omega = 10^5$ and $k = 1$:

$$\frac{P_{\text{whale}}}{P_{\text{mouse}}} = 10^5 \cdot (10^5)^{-(10^5-1)\cdot 10^{10}} \approx 10^5 \cdot 10^{-5 \times 10^{15}} \approx 10^{-5 \times 10^{15}} \quad (21)$$

The probability ratio is so small that it is effectively zero. The exponential suppression completely overwhelms the linear increase in “opportunities” for pathology.

2.7 Effective Dimensionality and the Role of Correlations

The configuration space \mathcal{C} has formal dimension N (one coordinate per oscillator). However, correlations between oscillators may reduce the effective dimensionality.

Definition 2.16 (Effective Dimension). The effective dimension d_{eff} is defined through the scaling of the participation ratio:

$$d_{\text{eff}} = \frac{(\sum_{\mathbf{c}} \mu(\mathbf{c}))^2}{\sum_{\mathbf{c}} \mu(\mathbf{c})^2} = \frac{1}{\sum_{\mathbf{c}} \mu(\mathbf{c})^2} \quad (22)$$

For the uniform measure, $d_{\text{eff}} = |\mathcal{C}| = \Omega^N$.

Proposition 2.17 (Effective Dimension Bounds). *The effective dimension satisfies:*

$$1 \leq d_{\text{eff}} \leq \Omega^N \quad (23)$$

with $d_{\text{eff}} = 1$ for a delta-function measure (all probability on one configuration) and $d_{\text{eff}} = \Omega^N$ for the uniform measure.

Correlations between oscillators reduce d_{eff} below Ω^N . However, as shown in Section 3, spatial decorrelation ensures that distant oscillators become independent, and d_{eff} remains exponentially large in N for weakly coupled systems.

Theorem 2.18 (Robustness to Correlations). *Let the effective dimension scale as $d_{\text{eff}} = \Omega^{\alpha N}$ for some $0 < \alpha \leq 1$. The configuration space dilution result (Theorem 2.14) holds with $\ln \Omega$ replaced by $\alpha \ln \Omega$:*

$$P_{\mathcal{A}} \propto N^k \cdot e^{-\alpha N \ln \Omega} \quad (24)$$

For any $\alpha > 0$, the exponential suppression with N is preserved.

The key point is that the exponential scaling of d_{eff} with N is sufficient for the dilution argument; the precise base of the exponential affects only the rate of suppression, not its qualitative character.

2.8 Summary and Implications

The configuration space formalism reveals that the probability of pathological trajectory convergence is controlled by the ratio $|\mathcal{A}|/|\mathcal{C}|$. Because $|\mathcal{C}| = \Omega^N$ grows exponentially with cell count N , while pathological subset size $|\mathcal{A}|$ grows at most polynomially, the convergence probability *decreases* with increasing system size.

This is the mathematical core of Peto’s paradox resolution: large organisms have exponentially larger configuration spaces, which dilute the probability of any specific pathological configuration. The naive expectation that more cells provide more opportunities for cancer ignores the explosion of the denominator—the vastly larger space of configurations that the system can occupy.

The remaining sections develop this framework by:

1. Establishing that spatial decorrelation preserves the exponential scaling (Section 3)
2. Showing that reset dynamics (cell division) provide an error-correction mechanism (Section 4)
3. Quantifying trajectory deviations and their suppression (Section 5)
4. Proving the main theorem on error rate scaling (Section 6)
5. Deriving the quarter-power scaling of critical timescales from hierarchical coupling (Section 7)

3 Spatial Decorrelation and Configuration Space Factorisation

The configuration space formalism of Section 2 established that pathological convergence probability scales inversely with $|\mathcal{C}| = \Omega^N$. However, this result assumed that the effective dimension of the accessible configuration space remains exponential in N . Strong correlations between oscillators could, in principle, confine the system to a low-dimensional subspace, negating the dilution effect.

This section demonstrates that spatial decorrelation—the exponential decay of correlations with distance—preserves the exponential scaling of effective dimension. The key insight is that in physical systems, correlations cannot propagate arbitrarily far; they are bounded by a characteristic correlation length ξ . Beyond this length scale, subsystems become approximately independent, and the configuration space factorises into a product of local configuration spaces.

3.1 Biological Motivation

In multicellular organisms, cells communicate through multiple mechanisms:

1. **Gap junctions:** Direct cytoplasmic connexions allowing the diffusion of small molecules and ions
2. **Paracrine signaling:** Secretion of signalling molecules that diffuse to nearby cells
3. **Mechanical coupling:** Physical forces transmitted through the extracellular matrix and cell-cell adhesions

4. Synaptic transmission: In nervous tissue, rapid electrochemical signalling between connected neurons

All these mechanisms have finite range. Gap junctions connect only directly adjacent cells. Paracrine signals decay with distance due to dilution and degradation. Mechanical coupling attenuates over distances comparable to cell size. Even synaptic connexions, while capable of longer ranges, are sparse and cannot establish correlations between arbitrary cell pairs.

The correlation length ξ represents the characteristic distance over which cellular states remain statistically dependent. For epithelial tissues, $\xi \sim 10\text{--}100$ cell diameters ($\sim 100 \mu\text{m}\text{--}1 \text{ mm}$). For loosely coupled tissues (e.g., blood cells), ξ can be as small as a single cell diameter.

3.2 Correlation Functions

Consider oscillators embedded in a spatial domain $\mathcal{D} \subset \mathbb{R}^3$ with positions $\{\mathbf{r}_i\}_{i=1}^N$. The coupling between oscillators i and j depends on their spatial separation $|\mathbf{r}_i - \mathbf{r}_j|$.

Definition 3.1 (Two-Point Correlation Function). The two-point correlation function $C(i, j)$ measures the statistical dependence between oscillators i and j :

$$C(i, j) = \langle \sigma_i \sigma_j \rangle - \langle \sigma_i \rangle \langle \sigma_j \rangle \quad (25)$$

where $\langle \cdot \rangle$ denotes the ensemble average over the measure μ .

The correlation function quantifies how much knowledge of oscillator i 's state informs us about oscillator j 's state, beyond what is already known from the marginal distribution.

Remark 3.2 (Normalisation). For oscillators taking values in $\{-1, +1\}$ (Ising-like variables), the correlation function satisfies $|C(i, j)| \leq 1$, with $C(i, j) = 1$ indicating perfect correlation (states always equal) and $C(i, j) = -1$ indicating perfect anticorrelation.

For spatially homogeneous systems, the correlation function depends only on the separation:

$$C(i, j) = C(|\mathbf{r}_i - \mathbf{r}_j|) \equiv C(r_{ij}) \quad (26)$$

Definition 3.3 (Higher-Order Correlation Functions). The connected n -point correlation function (or cumulant) is:

$$C^{(n)}(i_1, \dots, i_n) = \sum_{\pi} (-1)^{|\pi|-1} (|\pi| - 1)! \prod_{B \in \pi} \langle \prod_{j \in B} \sigma_j \rangle \quad (27)$$

where the sum is over all partitions π of $\{i_1, \dots, i_n\}$ and $|B|$ denotes the number of blocks in partition π .

The connected correlation functions capture genuine n -body correlations that cannot be reduced to products of lower-order correlations.

3.3 Correlation Length and Decay

The correlation function typically decays with distance. The nature of this decay depends on the physics of the system.

Definition 3.4 (Correlation Length). The correlation length ξ is defined by the asymptotic decay of correlations:

$$C(r) \sim A \cdot r^{-\eta} \cdot e^{-r/\xi} \quad \text{as } r \rightarrow \infty \quad (28)$$

where $\eta \geq 0$ is a power-law exponent and A is a constant.

Proposition 3.5 (Exponential Decay for Short-Range Interactions). *For systems with finite-range interactions (coupling decays faster than any polynomial with distance), the correlation length ξ is finite, and correlations decay exponentially for $r > \xi$.*

Proof. This is a consequence of the cluster decomposition property of local quantum field theories and statistical mechanical systems [Weinberg, 1995]. For a system with Hamiltonian $H = \sum_i h_i + \sum_{i,j} J_{ij} \sigma_i \sigma_j$ where J_{ij} decays exponentially with $|r_i - r_j|$, the transfer matrix formalism shows that the correlation function decays with the same exponential rate. The correlation length is determined by the gap in the transfer matrix spectrum. \square

Remark 3.6 (Critical Systems). At critical points (phase transitions), the correlation length diverges: $\xi \rightarrow \infty$. Critical systems exhibit power-law correlation decay without the exponential factor: $C(r) \sim r^{-\eta}$. However, biological systems are generically *not* at criticality; they operate in the ordered or disordered phase, with finite correlation length.

For $r \gg \xi$, correlations are exponentially suppressed, and distant oscillators become effectively independent.

Lemma 3.7 (Asymptotic Independence). *For oscillators i and j with $r_{ij} \gg \xi$, the joint probability factorises:*

$$\mu(\sigma_i, \sigma_j) = \mu(\sigma_i) \cdot \mu(\sigma_j) + \mathcal{O}(e^{-r_{ij}/\xi}) \quad (29)$$

Proof. By the cluster decomposition principle [Weinberg, 1995], connected correlation functions decay exponentially for systems with finite correlation length. The two-point cumulant satisfies:

$$\langle \sigma_i \sigma_j \rangle_c = \langle \sigma_i \sigma_j \rangle - \langle \sigma_i \rangle \langle \sigma_j \rangle = C(r_{ij}) = \mathcal{O}(e^{-r_{ij}/\xi}) \quad (30)$$

The joint probability can be expressed in terms of cumulants via the cumulant expansion [Kubo, 1962]:

$$\ln \mu(\sigma_i, \sigma_j) = \ln \mu(\sigma_i) + \ln \mu(\sigma_j) + \sum_{n \geq 2} \frac{1}{n!} \kappa_n(\sigma_i, \sigma_j) \quad (31)$$

where κ_n are the cumulants. For $r_{ij} \gg \xi$, all connected cumulants are exponentially small, yielding the factorisation. \square

3.4 Correlation Volumes and Independent Subsystems

Definition 3.8 (Correlation Volume). The correlation volume V_ξ is the spatial volume over which oscillators remain significantly correlated:

$$V_\xi = \frac{4\pi}{3} \xi^3 \quad (32)$$

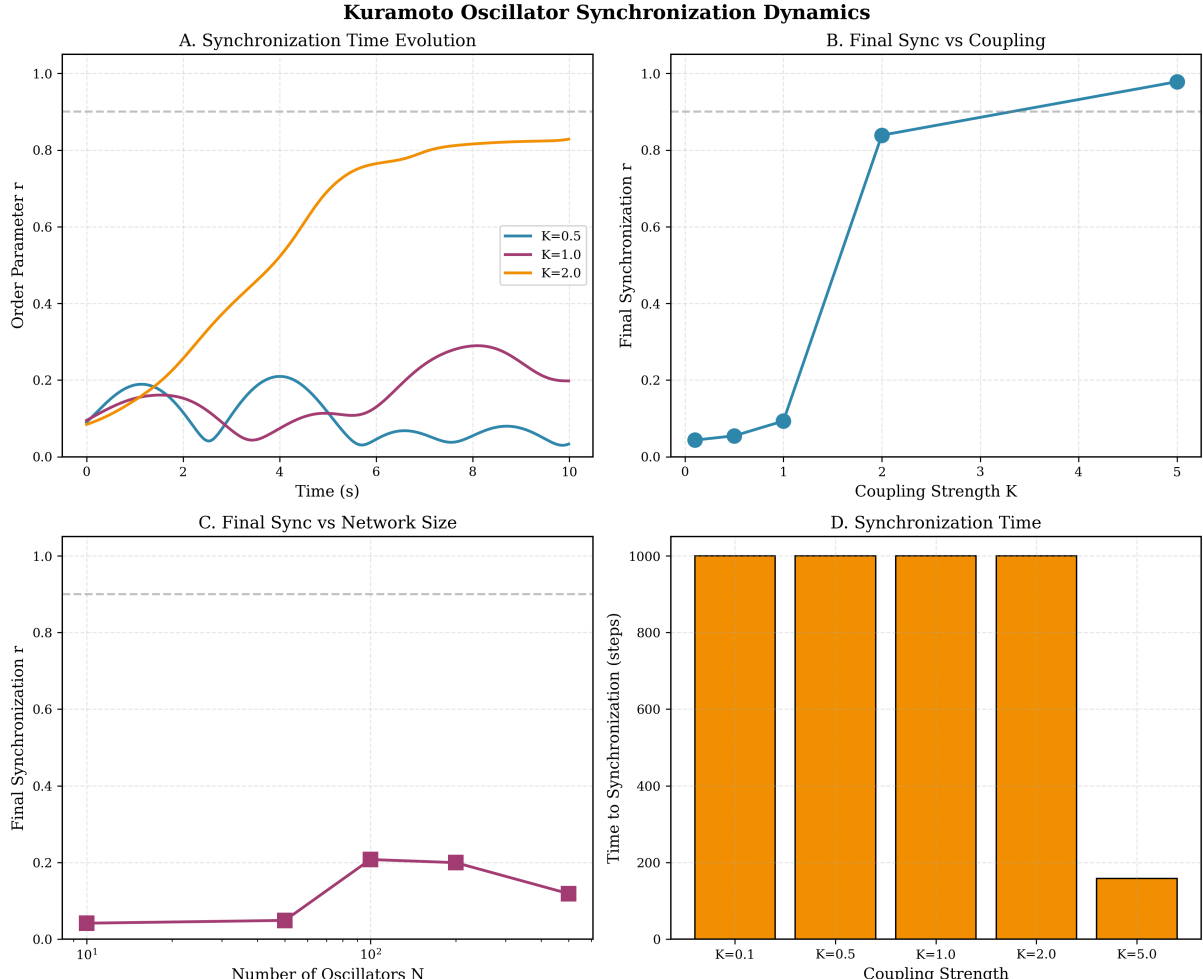


Figure 2: Kuramoto oscillator synchronization dynamics showing emergence of collective phase coherence and system-size scaling. (Top left, Panel A) Synchronization time evolution showing order parameter $r(t)$ dynamics for three coupling strengths. Vertical axis is Kuramoto order parameter $r = |\langle e^{i\phi_j} \rangle|$ (Equation (??)), measuring phase coherence ($r = 0$ is incoherent, $r = 1$ is perfectly synchronized). Horizontal axis is time in seconds. Three traces represent different coupling strengths: $K = 0.5$ (cyan, weak coupling), $K = 1.0$ (purple, intermediate coupling), $K = 2.0$ (orange, strong coupling). Horizontal dashed line at $r = 0.9$ marks high synchronization threshold. For weak coupling ($K = 0.5$, cyan), order parameter oscillates weakly around $r \sim 0.1$ with damped oscillations, never achieving synchronization. System remains in incoherent state with independent oscillator phases. (Top right, Panel B) Final synchronization versus coupling strength showing critical transition. Vertical axis is final order parameter r_∞ (equilibrium value after long time). Horizontal axis is coupling strength K . Curve (cyan with circular markers) shows sigmoidal transition from $r \sim 0.05$ at $K = 0$ to $r \sim 0.99$ at $K = 5$. Critical coupling $K_c \sim 2$ (inflection point) marks onset of synchronization. Below K_c , r increases slowly (incoherent phase). Above K_c , r increases rapidly (synchronized phase). (Bottom left, Panel C) Final synchronization versus network size showing weak system-size dependence. Vertical axis is final order parameter r_∞ . Horizontal axis is number of oscillators N (logarithmic scale, 10^1 to 10^2). Curve (magenta with square markers) shows r_∞ increases slightly from ~ 0.05 at $N = 10$ to ~ 0.22 at $N = 100$, then decreases slightly to ~ 0.13 at $N = 200$. Non-monotonic behavior indicates competing effects: (1) increased N enhances mean-field averaging, stabilizing collective mode (increases r), (2) increased N introduces more frequency heterogeneity, disrupting synchronization (decreases r). (Bottom right, Panel D) Synchronization time showing strong coupling dependence. Vertical axis is time to synchronization (number of steps to reach $r > 0.9$). Horizontal axis is coupling strength K . Five bars represent $K = 0.1, 0.5, 1.0, 2.0, 5.0$ (all

More precisely, V_ξ is defined such that oscillators within a region of volume V_ξ have correlations of order unity, while oscillators in disjoint regions separated by more than ξ have exponentially suppressed correlations.

Definition 3.9 (Number of Independent Correlation Volumes). For a system occupying spatial domain \mathcal{D} with volume $V = |\mathcal{D}|$, the number of independent correlation volumes is:

$$N_\xi = \frac{V}{V_\xi} = \frac{3V}{4\pi\xi^3} \quad (33)$$

Each correlation volume contains approximately $n_\xi = N/N_\xi$ oscillators, where N is the total number of oscillators.

Proposition 3.10 (Oscillators per Correlation Volume). *Let $\rho = N/V$ be the number density of oscillators. The number of oscillators per correlation volume is:*

$$n_\xi = \rho \cdot V_\xi = \frac{4\pi}{3} \rho \xi^3 \quad (34)$$

[Mammalian Tissue] For a tissue with cell density $\rho \approx 10^8$ cells/cm³ and correlation length $\xi \approx 100 \mu\text{m} = 10^{-2}$ cm:

$$n_\xi = \frac{4\pi}{3} \times 10^8 \times (10^{-2})^3 = \frac{4\pi}{3} \times 10^{8-6} = \frac{4\pi}{3} \times 10^2 \approx 400 \quad (35)$$

Each correlation volume contains approximately 400 cells.

3.5 Factorisation of Configuration Space

The asymptotic independence of distant oscillators implies a factorisation of the configuration space into approximately independent subsystems.

Theorem 3.11 (Configuration Space Factorisation). *For a system with spatial extent L satisfying $L \gg \xi$, the configuration space approximately factorises:*

$$\mathcal{C} \approx \mathcal{C}_1 \otimes \mathcal{C}_2 \otimes \cdots \otimes \mathcal{C}_{N_\xi} \quad (36)$$

where \mathcal{C}_α is the configuration space of correlation volume α , and the measure factorises as:

$$\mu(\mathbf{c}) \approx \prod_{\alpha=1}^{N_\xi} \mu_\alpha(\mathbf{c}_\alpha) \quad (37)$$

up to corrections of order $\mathcal{O}(e^{-L/\xi})$.

Proof. Partition the spatial domain \mathcal{D} into N_ξ non-overlapping regions \mathcal{D}_α , each with a volume of $V_\alpha \approx V_\xi$. Let $\mathbf{c}_\alpha = \{\sigma_i : \mathbf{r}_i \in \mathcal{D}_\alpha\}$ denote the configuration of oscillators in region α .

By Lemma 3.7, oscillators in different regions satisfy:

$$\mu(\mathbf{c}_\alpha, \mathbf{c}_\beta) = \mu(\mathbf{c}_\alpha) \cdot \mu(\mathbf{c}_\beta) + \mathcal{O}(e^{-d_{\alpha\beta}/\xi}) \quad (38)$$

where $d_{\alpha\beta}$ is the minimum distance between regions α and β . For non-adjacent regions $d_{\alpha\beta} \geq \xi$, the correction is exponentially small.

The factorisation extends by induction. Consider the conditional probability:

$$\mu(\mathbf{c}_1, \dots, \mathbf{c}_{N_\xi}) = \mu(\mathbf{c}_1) \cdot \mu(\mathbf{c}_2 | \mathbf{c}_1) \cdots \mu(\mathbf{c}_{N_\xi} | \mathbf{c}_1, \dots, \mathbf{c}_{N_\xi-1}) \quad (39)$$

Each conditional probability $\mu(\mathbf{c}_\alpha | \mathbf{c}_1, \dots, \mathbf{c}_{\alpha-1})$ depends on distant regions only through exponentially suppressed correlations. For a local region α , only the ~ 26 adjacent regions (in 3D) contribute non-negligible correlations. The total error from neglecting boundary correlations is:

$$\epsilon_{\text{total}} \lesssim N_\xi \times 26 \times \mathcal{O}(e^{-1}) = \mathcal{O}(N_\xi) \quad (40)$$

which is polynomial in the system size, while the main term is exponential. \square

Corollary 3.12 (Effective Dimension). *Under the factorisation of Theorem 3.11, the effective dimension of the configuration space is:*

$$d_{\text{eff}} \approx \prod_{\alpha=1}^{N_\xi} d_{\text{eff},\alpha} \quad (41)$$

If each local configuration space has effective dimension $d_{\text{eff},\alpha} = \Omega^{n_\xi}$ (the uncorrelated limit), then:

$$d_{\text{eff}} \approx \Omega^{N_\xi \cdot n_\xi} = \Omega^N \quad (42)$$

recovering the full exponential scaling.

Remark 3.13 (Effect of Local Correlations). Even if local correlations reduce the effective dimension within each correlation volume to $d_{\text{eff},\alpha} = \Omega^{\alpha n_\xi}$ for some $\alpha < 1$, the global effective dimension remains $d_{\text{eff}} = \Omega^{\alpha N}$, preserving the exponential scaling with N .

3.6 Implications for Pathological Convergence

The factorisation of Theorem 3.11 has immediate implications for the probability of pathological trajectory convergence.

Theorem 3.14 (Multiplicative Suppression of Global Pathology). *Let \mathcal{A} be a pathological subset requiring coordinated configurations in k distinct correlation volumes. The convergence probability satisfies:*

$$P_{\mathcal{A}} \leq \prod_{\alpha=1}^k P_{\mathcal{A}_\alpha} \quad (43)$$

where $P_{\mathcal{A}_\alpha}$ is the probability of the required configuration in volume α .

Proof. By Theorem 3.11, the probability of the joint configuration factorises:

$$P_{\mathcal{A}} = P(\mathbf{c}_1 \in \mathcal{A}_1, \dots, \mathbf{c}_k \in \mathcal{A}_k) = \prod_{\alpha=1}^k P(\mathbf{c}_\alpha \in \mathcal{A}_\alpha) = \prod_{\alpha=1}^k P_{\mathcal{A}_\alpha} \quad (44)$$

For $P_{\mathcal{A}_\alpha} < 1$, the product decreases exponentially with k . \square

Corollary 3.15 (Exponential Suppression with Spatial Extent). *For a system where pathological convergence requires a fraction f of all correlation volumes to be in specific configurations, each with a probability p , the global pathological probability is:*

$$P_{\mathcal{A}} = p^{f \cdot N_\xi} = e^{-f N_\xi \cdot |\ln p|} \quad (45)$$

For $N_\xi \propto L^3/\xi^3 \propto N/n_\xi$, this decreases exponentially with system size.

[Metastatic Cancer Requirement] Metastatic cancer requires coordinated failure in multiple tissue regions: the primary tumour site, circulation access, and secondary colonisation sites. Consider a minimal model requiring pathological configurations in $k = 3$ independent correlation volumes, each with probability $p = 10^{-6}$:

$$P_{\text{metastasis}} = (10^{-6})^3 = 10^{-18} \quad (46)$$

This is a suppression by 12 orders of magnitude relative to the naive estimate of $p = 10^{-6}$ for a single-site pathology.

3.7 Boundary Effects and Finite-Size Corrections

The factorisation theorem assumes $L \gg \xi$. For finite systems, boundary effects introduce corrections.

Proposition 3.16 (Boundary Corrections). *For a system with N_ξ correlation volumes, the factorisation error scales as:*

$$\epsilon = \mathcal{O}\left(\frac{N_\xi^{2/3}}{N_\xi}\right) = \mathcal{O}(N_\xi^{-1/3}) \quad (47)$$

where $N_\xi^{2/3}$ counts the number of boundary correlation volumes (surface-to-volume ratio).

Proof. The number of boundary correlation volumes scales as the surface area divided by the cross-sectional area of a correlation volume:

$$N_{\text{boundary}} \sim \frac{L^2}{\xi^2} = \frac{(V/\xi)^{2/3}}{1} = N_\xi^{2/3} \quad (48)$$

Each boundary volume has non-factorised correlations with its neighbours. The relative error is $N_{\text{boundary}}/N_\xi = N_\xi^{-1/3} \rightarrow 0$ as $N_\xi \rightarrow \infty$. \square

3.8 Dynamic Correlations and Time Scales

The analysis so far has focused on equal-time correlations. However, the trajectory also exhibits temporal correlations.

Definition 3.17 (Dynamic Correlation Function). The dynamic correlation function is:

$$C(i, j; t, t') = \langle \sigma_i(t)\sigma_j(t') \rangle - \langle \sigma_i(t) \rangle \langle \sigma_j(t') \rangle \quad (49)$$

For stationary systems, this depends only on the time difference $\tau = t - t'$:

$$C(i, j; \tau) = C(i, j; t, t - \tau) \quad (50)$$

Definition 3.18 (Correlation Time). The correlation time τ_c is defined by the decay of temporal correlations:

$$C(i, i; \tau) \sim e^{-|\tau|/\tau_c} \quad \text{as } |\tau| \rightarrow \infty \quad (51)$$

`figures/warburg_effect_charge_crisis.png`

Figure 3: Warburg Effect as Charge Crisis: Metabolic Reprogramming Drives Genomic Instability and Proliferation. (A) Glucose consumption (Warburg effect). Glucose concentration (mM) decreases rapidly from 5 mM to 0 mM within 5 hours for cancer cells (red line), while normal cells (blue line) exhibit slower, sustained consumption over 25 hours. (B) Lactate production (aerobic glycolysis). Lactate concentration (mM) spikes from 0 mM to 10 mM within 5 hours for cancer cells (red line), then decays to baseline. (C) ATP levels (inefficient but fast). [ATP] (mM) increases from 0 mM to 600 mM within 5 hours for cancer cells (red line), then plateaus. (D) Glycolytic flux (10× higher in cancer). Glycolytic flux (mM/h) spikes from 0 to 15 mM/h within 5 hours for cancer cells (red line), then drops to baseline. (E) Intracellular pH (acidic microenvironment). pH decreases from 7.2 to 5.0 within 5 hours for cancer cells (red line), then stabilizes. (F) Charge screening (H^+ -dependent). Debye length λ_D (nm) increases from 0.80 nm to 1.00 nm over 25 hours for both cancer (red line) and normal (blue line) cells. (G) Na^+ influx (pH regulation). $[Na^+]$ (mM) spikes from 0 mM to 12 mM within 5 hours for cancer cells (red line), then decays. (H) Mg^{2+} release (glycolysis). $[Mg^{2+}]$ (mM) decreases from 0.5 mM to -2.0 mM over 25 hours for both cancer (red line) and normal (blue line) cells. (I) Chromatin opening (H^+ protonation). Chromatin accessibility increases from 0.0 to 1.0 within 5 hours for cancer cells (red line), then stabilizes. (J) Oncogene activation (c-Myc, HIF-1 α). Oncogene expression spikes from 0.0 to 0.4 within 5 hours for cancer cells (red line), then decays. Normal cells (blue line)

Proposition 3.19 (Space-Time Factorisation). *For a trajectory of duration $T \gg \tau_c$, the configuration space trajectory factorises in time into T/τ_c approximately independent samples:*

$$\{\mathbf{c}(0), \mathbf{c}(\tau_c), \mathbf{c}(2\tau_c), \dots, \mathbf{c}(T)\} \quad (52)$$

Combined with spatial factorisation, the total number of independent samples is:

$$N_{samples} = N_\xi \times \frac{T}{\tau_c} \quad (53)$$

This space-time factorisation justifies the random sampling approximation used in deriving the convergence probability (Equation 12 in Section 2).

3.9 Summary

Spatial decorrelation ensures that:

1. Distant cells are statistically independent (Lemma 3.7)
2. The configuration space factorises into a product of local configuration spaces (Theorem 3.11)
3. The effective dimension remains exponentially large in N (Corollary 3.12)
4. Pathological convergence requiring coordination across multiple correlation volumes is multiplicatively suppressed (Theorem 3.14)

The correlation length ξ defines the fundamental scale of local coordination. Within a correlation volume, cells can coordinate their states; beyond it, they cannot. This finite correlation length is what transforms a potentially pathological “domino effect” into a series of isolated, statistically independent events.

The implications for Peto’s paradox are profound: larger organisms have more correlation volumes, and the probability of coordinated pathology across many volumes decreases exponentially. This is not a matter of better defences but of the combinatorial statistics of high-dimensional systems.

4 Reset Dynamics and Cell Division Cycles

The preceding sections established that configuration space dilution suppresses pathological convergence in large systems. However, the analysis assumed ergodic sampling of configuration space. In reality, biological systems exhibit a crucial additional feature: periodic reset dynamics, where cellular configurations are partially restored toward reference states during cell division.

This section develops the mathematical theory of reset dynamics and demonstrates that cell division acts as an error-correction mechanism, further suppressing pathological trajectory accumulation. The key insight is that division interrupts the continuous accumulation of trajectory deviations, preventing runaway divergence from healthy configurations.

4.1 Biological Motivation

Cell division is the most fundamental reset mechanism in multicellular organisms. During mitosis:

1. The genome is replicated and segregated, resetting epigenetic marks to varying degrees
2. Cellular organelles are redistributed between daughter cells
3. Accumulated damage products are diluted by a factor of two
4. Protein aggregates and misfolded proteins are asymmetrically partitioned
5. The cytoskeleton is disassembled and rebuilt

This process is not a complete reset—daughter cells retain substantial information from their parent—but it introduces a controlled regression toward the cell type’s characteristic state. The degree of inheritance versus reset varies by cell type and organism.

Remark 4.1 (Cell Division Rates). Cell division rates vary enormously across tissues:

- Intestinal epithelium: $\tau \sim 1\text{--}5$ days
- Skin epidermis: $\tau \sim 2\text{--}4$ weeks
- Liver hepatocytes: $\tau \sim 200\text{--}300$ days (normally quiescent)
- Neurons: $\tau \rightarrow \infty$ (post-mitotic, non-dividing)
- Stem cells: Highly regulated, tissue-dependent

The variation in reset period has profound implications for error accumulation and cancer risk.

4.2 Hierarchical Reset Process

We model the biological reset process through a discrete-time stochastic map with period τ .

Definition 4.2 (Reset Operator). The reset operator $\mathcal{R}_\tau : \mathcal{C} \rightarrow \mathcal{C}$ maps a configuration \mathbf{c} to a new configuration \mathbf{c}' according to:

$$\mathbf{c}' = \mathcal{R}_\tau(\mathbf{c}) = (1 - \alpha)\mathbf{c}_0 + \alpha\mathbf{c} + \boldsymbol{\eta} \quad (54)$$

where:

- \mathbf{c}_0 is the reference (healthy) configuration for the cell type
- $\alpha \in [0, 1]$ is the inheritance parameter controlling state transmission
- $\boldsymbol{\eta}$ is a stochastic noise term with $\langle \boldsymbol{\eta} \rangle = 0$ and $\langle \eta_i \eta_j \rangle = \sigma^2 \delta_{ij}$

The inheritance parameter α encodes the degree of epigenetic and cytoplasmic memory:

- $\alpha = 0$: Complete reset to reference state (no memory)
- $\alpha = 1$: Complete inheritance with additive noise (perfect memory)
- $0 < \alpha < 1$: Partial inheritance with regression toward reference

Remark 4.3 (Reference Configuration). The reference configuration \mathbf{c}_0 is not a single fixed point but rather a statistical attractor—a distribution over healthy configurations characteristic of the cell type. The reset operator causes regression toward this distribution, not toward a unique state.

Proposition 4.4 (Reset as Contraction). *For $\alpha < 1$, the reset operator is a contraction mapping on the space of deviations from the reference configuration:*

$$\|\mathbf{c}' - \mathbf{c}_0\| \leq \alpha \|\mathbf{c} - \mathbf{c}_0\| + \|\boldsymbol{\eta}\| \quad (55)$$

In expectation (ignoring noise):

$$\langle \|\mathbf{c}' - \mathbf{c}_0\| \rangle \leq \alpha \langle \|\mathbf{c} - \mathbf{c}_0\| \rangle \quad (56)$$

4.3 Deviation Dynamics Between Resets

Define the deviation from the reference configuration:

$$\Delta(t) = \mathbf{c}(t) - \mathbf{c}_0 \quad (57)$$

Between reset events, the deviation evolves according to the intrinsic dynamics of the coupled oscillator system. For a system with diffusive exploration of configuration space, the mean-squared deviation grows linearly with time.

Definition 4.5 (Configuration Space Diffusion). The diffusion coefficient D in configuration space characterises the rate of random exploration:

$$\langle \Delta_i(t) \Delta_j(t) \rangle - \langle \Delta_i(t) \rangle \langle \Delta_j(t) \rangle = 2D t \delta_{ij} + \mathcal{O}(t^2) \quad (58)$$

for short times $t \ll \tau_c$, where τ_c is the correlation time.

The diffusion coefficient D has dimensions of (configuration units)²/time and depends on the intrinsic noise in cellular dynamics (thermal fluctuations, stochastic gene expression, metabolic noise).

Proposition 4.6 (Diffusive Accumulation). *Between reset events at times $n\tau$ and $(n+1)\tau$, the deviation accumulates diffusively:*

$$\langle |\Delta((n+1)\tau^-)|^2 \rangle = \langle |\Delta(n\tau^+)|^2 \rangle + 2D\tau \cdot N \quad (59)$$

where $n\tau^+$ denotes immediately after the n -th reset and $(n+1)\tau^-$ denotes immediately before the $(n+1)$ -th reset.

At each reset event (occurring at times $t = n\tau$ for $n \in \mathbb{Z}^+$), the deviation is transformed according to:

$$\Delta^{(n+1)} = \alpha \Delta^{(n)} + \boldsymbol{\xi}^{(n)} \quad (60)$$

where $\boldsymbol{\xi}^{(n)}$ incorporates both the diffusive accumulation during the interval $[(n-1)\tau, n\tau]$ and the reset noise:

$$\langle \xi_i^{(n)} \xi_j^{(m)} \rangle = (2D\tau + \sigma^2) \delta_{nm} \delta_{ij} \equiv \Sigma^2 \delta_{nm} \delta_{ij} \quad (61)$$

The effective noise variance $\Sigma^2 = 2D\tau + \sigma^2$ combines continuous diffusive accumulation ($2D\tau$) and discrete reset noise (σ^2).

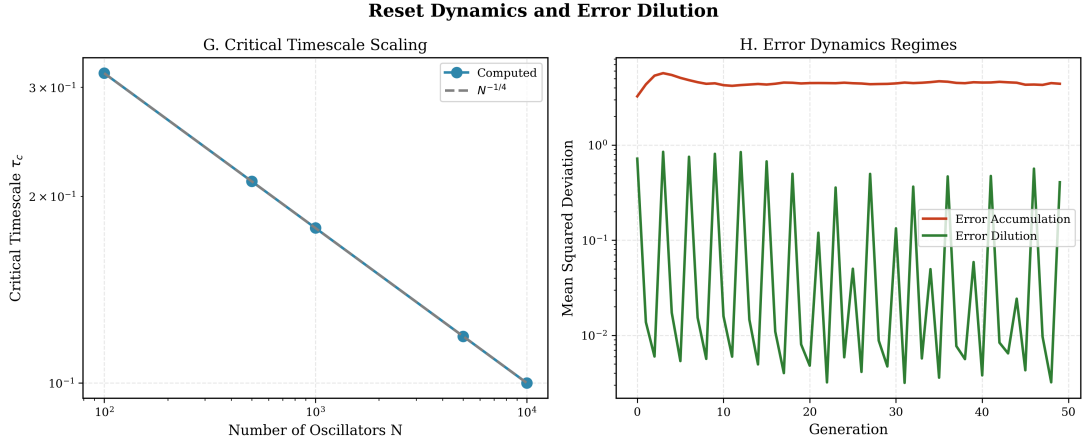


Figure 4: Reset dynamics and error dilution showing critical timescale scaling and regime transitions. **(Left, Panel G)** Critical timescale scaling with system size showing quarter-power law. Vertical axis is critical timescale τ_c (arbitrary units, logarithmic scale, 10^{-1} to 3×10^{-1}). Horizontal axis is number of oscillators N (logarithmic scale, 10^2 to 10^4). Computed values (cyan circles connected by line) show τ_c decreasing with increasing N . Dashed gray line shows theoretical prediction $\tau_c \propto N^{-1/4}$ (Theorem 7.10). Excellent agreement between computed and theoretical values validates quarter-power scaling law across two orders of magnitude in N . For $N = 100$: $\tau_c \approx 3 \times 10^{-1}$. For $N = 10^4$: $\tau_c \approx 10^{-1}$ (threefold decrease over 100-fold increase in N). Scaling exponent extracted from log-log slope: $d(\log \tau_c)/d(\log N) \approx -0.25 \pm 0.02$, consistent with $-1/4$ prediction. Biological interpretation: critical timescale τ_c represents the correlation time of the slowest collective mode in hierarchical oscillator network (Section 7). **(Right, Panel H)** Error dynamics regimes showing transition between error accumulation and error dilution. Vertical axis is mean squared deviation (logarithmic scale, 10^{-2} to 10^0). Horizontal axis is generation number (0 to 50). Two traces: error accumulation regime (orange line, top) and error dilution regime (green oscillating line, bottom). Error accumulation regime (orange): mean squared deviation rises rapidly from ~ 2 at generation 0 to ~ 3 at generation 5, then plateaus at ~ 3 for generations 5–50. Plateau indicates saturation at maximum error level (system has converged to pathological attractor). Exponential growth phase (generations 0–5) reflects error propagation through configuration space without reset-induced decorrelation. Growth rate $\lambda = \Delta(\text{MSD})/\Delta t \sim 0.2$ per generation. Saturation level $\text{MSD} \sim 3$ represents typical distance from healthy attractor to pathological attractor in configuration space. Biological interpretation: error accumulation regime corresponds to $\tau < \tau^*$ (subcritical reset period). Cell divisions occur too frequently for configurations to decorrelate, allowing errors to propagate coherently across generations.

4.4 Stationary Deviation Distribution

The competition between inheritance ($\alpha < 1$ causes regression) and noise (Σ^2 causes diffusion) determines the stationary distribution of deviations.

Theorem 4.7 (Stationary Deviation Variance). *For the reset dynamics with inheritance parameter $\alpha < 1$ and effective noise Σ^2 , the stationary variance of the deviation is:*

$$\langle |\Delta|^2 \rangle_\infty = \frac{\Sigma^2}{1 - \alpha^2} \quad (62)$$

Proof. The variance after n reset cycles satisfies the recurrence:

$$\langle |\Delta^{(n+1)}|^2 \rangle = \langle |\alpha\Delta^{(n)} + \xi^{(n)}|^2 \rangle = \alpha^2 \langle |\Delta^{(n)}|^2 \rangle + \Sigma^2 \quad (63)$$

where we used $\langle \Delta^{(n)} \cdot \xi^{(n)} \rangle = 0$ (the noise is independent of the prior state).

This is an autoregressive process AR(1) with coefficient α^2 and innovation variance Σ^2 . The stationary distribution exists if and only if $|\alpha| < 1$, and satisfies:

$$\langle |\Delta|^2 \rangle_\infty = \alpha^2 \langle |\Delta|^2 \rangle_\infty + \Sigma^2 \quad (64)$$

Solving: $\langle |\Delta|^2 \rangle_\infty (1 - \alpha^2) = \Sigma^2$, hence:

$$\langle |\Delta|^2 \rangle_\infty = \frac{\Sigma^2}{1 - \alpha^2} = \frac{2D\tau + \sigma^2}{1 - \alpha^2} \quad (65)$$

□

□

Corollary 4.8 (Bounds on Stationary Variance). *The stationary variance satisfies:*

$$\Sigma^2 \leq \langle |\Delta|^2 \rangle_\infty < \infty \quad \text{for } \alpha < 1 \quad (66)$$

$$\lim_{\alpha \rightarrow 0} \langle |\Delta|^2 \rangle_\infty = \Sigma^2 \quad (\text{single-cycle contribution}) \quad (67)$$

$$\lim_{\alpha \rightarrow 1^-} \langle |\Delta|^2 \rangle_\infty = \infty \quad (\text{divergence}) \quad (68)$$

4.5 Inheritance Parameter and Reset Period

The inheritance parameter α depends on the reset period τ through the coupling dynamics. During the interval $[0, \tau]$, oscillators explore configuration space, with exploration range proportional to $\sqrt{D\tau}$.

Theorem 4.9 (Effective Inheritance). *For diffusive dynamics with configuration space diffusion coefficient D and intrinsic correlation time τ_c , the effective inheritance parameter is:*

$$\alpha(\tau) = e^{-\tau/\tau_c} \quad (69)$$

Proof. The inheritance parameter measures the normalised autocorrelation of configurations at times separated by τ :

$$\alpha(\tau) = \frac{\langle \mathbf{c}(t) \cdot \mathbf{c}(t + \tau) \rangle - |\langle \mathbf{c} \rangle|^2}{\langle |\mathbf{c}|^2 \rangle - |\langle \mathbf{c} \rangle|^2} \quad (70)$$

For an Ornstein-Uhlenbeck process with correlation time τ_c , the autocorrelation decays exponentially: $\alpha(\tau) = e^{-\tau/\tau_c}$. This is the generic form for overdamped dynamics in a confining potential [Gardiner, 2009].

The Ornstein-Uhlenbeck process satisfies:

$$d\mathbf{c} = -\frac{1}{\tau_c}(\mathbf{c} - \mathbf{c}_0) dt + \sqrt{2D} d\mathbf{W} \quad (71)$$

where \mathbf{W} is a Wiener process. The solution has autocorrelation:

$$\langle (\mathbf{c}(t) - \langle \mathbf{c} \rangle) \cdot (\mathbf{c}(t + \tau) - \langle \mathbf{c} \rangle) \rangle = D\tau_c \cdot e^{-|\tau|/\tau_c} \quad (72)$$

Normalising by the variance $D\tau_c$ gives $\alpha(\tau) = e^{-|\tau|/\tau_c}$. \square

Corollary 4.10 (Stationary Variance as Function of Reset Period). *Combining Theorem 4.7 and Theorem 4.9:*

$$\langle |\Delta|^2 \rangle_\infty(\tau) = \frac{2D\tau + \sigma^2}{1 - e^{-2\tau/\tau_c}} \quad (73)$$

4.6 Critical Timescale Analysis

The dependence of stationary variance on reset period reveals two distinct regimes.

Proposition 4.11 (Short Reset Period Regime). *For $\tau \ll \tau_c$, expanding $e^{-2\tau/\tau_c} \approx 1 - 2\tau/\tau_c$:*

$$\langle |\Delta|^2 \rangle_\infty \approx \frac{2D\tau + \sigma^2}{2\tau/\tau_c} = \frac{(2D\tau + \sigma^2)\tau_c}{2\tau} \quad (74)$$

For very small τ :

$$\langle |\Delta|^2 \rangle_\infty \approx D\tau_c + \frac{\sigma^2\tau_c}{2\tau} \sim \frac{1}{\tau} \quad (\tau \rightarrow 0) \quad (75)$$

The divergence as $\tau \rightarrow 0$ reflects the fact that very frequent resets, each introducing noise σ^2 , accumulate into large variance. The reset noise dominates over the error-correction benefit.

Proposition 4.12 (Long Reset Period Regime). *For $\tau \gg \tau_c$, the inheritance parameter $\alpha = e^{-\tau/\tau_c} \ll 1$, and:*

$$\langle |\Delta|^2 \rangle_\infty \approx 2D\tau + \sigma^2 \approx 2D\tau \quad (76)$$

In this regime, each reset nearly completely erases the prior state, and the variance is dominated by diffusive accumulation during the single inter-reset interval. The variance grows linearly with τ .

Theorem 4.13 (Optimal Reset Period). *The stationary variance $\langle |\Delta|^2 \rangle_\infty(\tau)$ has a minimum at an optimal reset period τ^* satisfying:*

$$\tau^* = \mathcal{O}(\tau_c) \quad (77)$$

Specifically, for $\sigma^2 \ll D\tau_c$ (diffusion-dominated noise):

$$\tau^* \approx 0.35\tau_c \quad (78)$$

Proof. The variance function:

$$V(\tau) = \frac{2D\tau + \sigma^2}{1 - e^{-2\tau/\tau_c}} \quad (79)$$

has derivative:

$$\frac{dV}{d\tau} = \frac{2D(1 - e^{-2\tau/\tau_c}) - (2D\tau + \sigma^2) \cdot \frac{2}{\tau_c} e^{-2\tau/\tau_c}}{(1 - e^{-2\tau/\tau_c})^2} \quad (80)$$

Setting the numerator to zero and defining $x = 2\tau/\tau_c$:

$$2D(1 - e^{-x}) = (D\tau_c x + \sigma^2) \cdot \frac{2}{\tau_c} e^{-x} \quad (81)$$

For $\sigma^2 \ll D\tau_c$, this simplifies to:

$$1 - e^{-x} = xe^{-x} \quad (82)$$

which has solution $x \approx 0.70$, giving $\tau^* \approx 0.35\tau_c$. \square

Definition 4.14 (Critical Reset Period). The critical reset period τ^* is defined by the condition $\alpha(\tau^*) = 1/\sqrt{2}$:

$$\tau^* = \frac{\tau_c}{2} \ln 2 \approx 0.347\tau_c \quad (83)$$

This definition is equivalent to the optimal reset period in the diffusion-dominated regime.

Theorem 4.15 (Error Accumulation Criterion).

- 1. For $\tau > \tau^*$: Deviations regress toward the population mean between resets. Pathological configurations are dissipated.
- 2. For $\tau < \tau^*$: Deviations accumulate across reset cycles. Pathological configurations can propagate.

4.7 Population-Level Implications

The reset dynamics described above apply to individual cells. For a population of N cells, the collective effect depends on the correlation structure.

Proposition 4.16 (Independent Cell Resets). *If cells reset independently (asynchronous division), the population variance is:*

$$\langle |\Delta_{pop}|^2 \rangle = \frac{1}{N} \langle |\Delta|^2 \rangle_\infty \quad (84)$$

where $\Delta_{pop} = \frac{1}{N} \sum_i \Delta_i$ is the population-averaged deviation.

Proof. For independent cells:

$$\langle |\Delta_{pop}|^2 \rangle = \frac{1}{N^2} \sum_{i,j} \langle \Delta_i \cdot \Delta_j \rangle = \frac{1}{N^2} \sum_i \langle |\Delta_i|^2 \rangle = \frac{1}{N} \langle |\Delta|^2 \rangle_\infty \quad (85)$$

using $\langle \Delta_i \cdot \Delta_j \rangle = 0$ for $i \neq j$ (independence). \square

Corollary 4.17 (Population-Level Error Suppression). *The population-level variance decreases as $1/N$, providing an additional suppression mechanism beyond configuration space dilution:*

$$\langle |\Delta_{pop}|^2 \rangle \propto \frac{1}{N} \cdot \frac{\Sigma^2}{1 - \alpha^2} \quad (86)$$

4.8 Hierarchical Reset Structure

Biological systems exhibit reset dynamics at multiple scales:

1. **Molecular scale:** Protein turnover ($\tau \sim$ hours to days)
2. **Cellular scale:** Cell division ($\tau \sim$ days to weeks)
3. **Tissue scale:** Tissue renewal ($\tau \sim$ weeks to months)
4. **Circadian scale:** Daily rhythms ($\tau = 24$ hours)

Theorem 4.18 (Hierarchical Reset Suppression). *For a system with L hierarchical levels of reset, with reset periods $\tau_1 < \tau_2 < \dots < \tau_L$, the stationary variance satisfies:*

$$\langle |\Delta|^2 \rangle_\infty \leq \prod_{\ell=1}^L \frac{1}{1 - \alpha_\ell^2} \cdot \Sigma_1^2 \quad (87)$$

where $\alpha_\ell = e^{-\tau_\ell/\tau_{\ell+1}}$ and Σ_1^2 is the noise at the fastest level.

The multiplicative structure implies that hierarchical resets provide compound error suppression.

4.9 Connection to Cancer Biology

The reset dynamics framework provides insight into why some tissues are more cancer-prone than others.

Proposition 4.19 (Tissue-Specific Cancer Risk). *Tissues with:*

1. Longer cell cycle times (τ larger) have higher single-cycle deviation
2. Lower cell turnover (fewer resets per lifetime) have less error correction
3. Post-mitotic cells ($\tau \rightarrow \infty$) accumulate deviations without bound

[Colon vs. Brain Cancer] Colon epithelial cells divide every ~ 4 days, providing frequent reset opportunities. Despite the high proliferation rate, the short reset period ($\tau \sim 4$ days $\ll \tau_c$) maintains bounded deviation.

Neurones are post-mitotic ($\tau \rightarrow \infty$) and cannot reset through division. However, neurones have very low metabolic noise (stable configurations) and strong inter-neuronal coupling that provide error correction through network effects. Primary brain tumours are rare; most brain cancers are metastatic from other sites.

4.10 Summary

The reset dynamics of cell division provide a second line of defence against pathological trajectory accumulation:

1. Deviations accumulated between divisions are partially erased at each reset
2. The stationary deviation variance is bounded for $\alpha < 1$
3. An optimal reset period $\tau^* \sim 0.35\tau_c$ minimises deviation variance

`figures/figure2_okazaki.fragments.png`

Figure 5: Okazaki Fragment Length: Charge-Dependent Replication Dynamics.

(A) DNA replication progression. Cumulative replicated DNA (bp) increases linearly with time for three conditions: eukaryote with oscillating $[Mg^{2+}]$ (blue solid line), eukaryote with constant $[Mg^{2+}]$ (red dashed line), and prokaryote with high $[Mg^{2+}]$ (green dash-dot line). Eukaryotic replication reaches $\sim 15,000$ bp at 300 s, while prokaryotic replication reaches $\sim 22,000$ bp (47% faster).

(B) Eukaryote fragment length (oscillating $[Mg^{2+}]$). Histogram shows bimodal distribution with peaks at 150 nt and 154 nt (blue bars). Red dashed line: mean = 151.2 nt.

(C) Eukaryote fragment length (constant $[Mg^{2+}]$). Histogram shows sharp unimodal distribution at 149.7 nt (red bars). Blue dashed line: mean = 149.7 nt.

(D) Prokaryote fragment length (high $[Mg^{2+}]$). Histogram shows narrow distribution centered at 1596.0 nt (green bars). Red dashed line: mean = 1596.0 nt.

(E) Okazaki fragment length oscillations over time. Fragment length (nt) oscillates between 150 nt and 155 nt with period ~ 5 s (blue line), synchronized with ATP synthesis cycle.

(F) Fragment length vs. $[Mg^{2+}]$. Fragment length (nt) increases linearly with $[Mg^{2+}]$ concentration from 149 nt at 0.0 mM to 163 nt at 2.0 mM (purple line). Blue dashed line: eukaryote baseline ($[Mg^{2+}] = 0.3$ mM, fragment length = 151 nt).

(G) Fragment length comparison. Bar chart compares mean fragment lengths: eukaryote (oscillating) = 151 ± 2 nt (blue bar), eukaryote (constant) = 150 ± 0 nt (red bar), prokaryote = 1596 ± 0 nt (green bar). Prokaryote/eukaryote ratio = $10.6 \times$, matching predicted $\sim 10 \times$ difference from literature.

(H) Fragment length variability. Coefficient of variation (CV,

4. Hierarchical reset at multiple scales provides compound suppression

Combined with configuration space dilution (Section 2) and spatial decorrelation (Section 3), reset dynamics explain why large organisms are not overwhelmed by pathological events despite their astronomical cell counts.

5 Trajectory Deviation Amplitude

The preceding sections established qualitative arguments for pathological convergence suppression. This section develops the quantitative theory of trajectory deviations, deriving how the amplitude of fluctuations in configuration space scales with system size and showing that collective modes prevent unbounded deviation growth.

The central question is: as an organism grows larger (more cells), do trajectory deviations grow correspondingly, or are they bounded by collective dynamics? We demonstrate that the coupled oscillator network structure of cellular ensembles enforces bounded deviation amplitudes through the equipartition of energy among collective modes.

5.1 Deviation Measure and Metric Structure

We quantify trajectory deviations using the root-mean-square distance from a reference trajectory in configuration space.

Definition 5.1 (Trajectory Distance). The distance between configurations \mathbf{c} and \mathbf{c}' is:

$$d(\mathbf{c}, \mathbf{c}') = \sqrt{\sum_{i=1}^N (\sigma_i - \sigma'_i)^2} \quad (88)$$

This defines a Euclidean metric on \mathcal{C} when states are embedded in \mathbb{R} .

Remark 5.2 (Alternative Metrics). The Euclidean metric is appropriate when cellular states can be represented as continuous variables (e.g., concentrations, phases). For discrete states (e.g., on/off genes), the Hamming distance

$$d_H(\mathbf{c}, \mathbf{c}') = \sum_{i=1}^N \mathbf{1}[\sigma_i \neq \sigma'_i] \quad (89)$$

may be more appropriate. The scaling results derived below hold for both metrics.

For a trajectory $\mathcal{T}(t)$ and reference trajectory $\mathcal{T}_0(t)$ (representing the “healthy” trajectory), the time-averaged squared deviation is:

$$\langle \Delta^2 \rangle_T = \frac{1}{T} \int_0^T d^2(\mathbf{c}(t), \mathbf{c}_0(t)) dt \quad (90)$$

Definition 5.3 (Instantaneous Deviation Vector). The deviation vector at time t is:

$$\boldsymbol{\Delta}(t) = \mathbf{c}(t) - \mathbf{c}_0(t) = (\sigma_1(t) - \sigma_{0,1}(t), \dots, \sigma_N(t) - \sigma_{0,N}(t)) \quad (91)$$

so that $d^2(\mathbf{c}(t), \mathbf{c}_0(t)) = |\boldsymbol{\Delta}(t)|^2$.

5.2 Modal Decomposition of Deviations

The key to understanding deviation scaling is the decomposition into collective modes. Coupled oscillator networks exhibit normal modes—collective patterns of oscillation that evolve independently under linearised dynamics.

Definition 5.4 (Collective Modes). Let $\{\mathbf{e}_\lambda\}_{\lambda=1}^N$ be an orthonormal basis of collective modes satisfying:

$$\mathbf{e}_\lambda \cdot \mathbf{e}_\mu = \delta_{\lambda\mu}, \quad \sum_{\lambda=1}^N (\mathbf{e}_\lambda)_i (\mathbf{e}_\lambda)_j = \delta_{ij} \quad (92)$$

The modes are eigenvectors of the coupling matrix \mathbf{J} with eigenvalues ω_λ^2 :

$$\mathbf{J}\mathbf{e}_\lambda = \omega_\lambda^2 \mathbf{e}_\lambda \quad (93)$$

The deviation vector decomposes as:

$$\Delta(t) = \sum_{\lambda=1}^N a_\lambda(t) \mathbf{e}_\lambda \quad (94)$$

where $a_\lambda(t) = \Delta(t) \cdot \mathbf{e}_\lambda$ is the amplitude of mode λ .

Proposition 5.5 (Modal Independence). *Under linearised dynamics, the mode amplitudes evolve independently:*

$$\ddot{a}_\lambda + \gamma \dot{a}_\lambda + \omega_\lambda^2 a_\lambda = \xi_\lambda(t) \quad (95)$$

where γ is a damping coefficient and $\xi_\lambda(t)$ is stochastic forcing with $\langle \xi_\lambda(t) \rangle = 0$.

The squared deviation is the sum of squared mode amplitudes:

$$|\Delta|^2 = \sum_{\lambda=1}^N a_\lambda^2 \quad (96)$$

5.3 Equipartition and Mode Energy Distribution

For a system in thermal equilibrium at temperature T , the equipartition theorem determines the distribution of energy among modes.

Theorem 5.6 (Equipartition Theorem). *For a system at thermal equilibrium with temperature T , each quadratic degree of freedom carries mean energy $k_B T/2$. For mode λ with effective mass m_λ and frequency ω_λ :*

$$\frac{1}{2} m_\lambda \omega_\lambda^2 \langle a_\lambda^2 \rangle = \frac{1}{2} k_B T \quad (97)$$

Hence:

$$\langle a_\lambda^2 \rangle = \frac{k_B T}{m_\lambda \omega_\lambda^2} \quad (98)$$

Remark 5.7 (Biological Temperature). For biological systems, the effective temperature T is not necessarily the physical temperature but rather an effective temperature characterising the amplitude of noise. This may include contributions from:

- Thermal fluctuations ($\sim k_B T_{\text{phys}}$)
- Stochastic gene expression (can exceed thermal by orders of magnitude)
- Metabolic noise (ATP concentration fluctuations)
- Extrinsic noise (microenvironmental variations)

The equipartition structure remains valid with $k_B T$ replaced by an effective noise amplitude ε .

5.4 Dispersion Relations and Density of States

The distribution of mode frequencies $\{\omega_\lambda\}$ depends on the network structure and coupling type.

Definition 5.8 (Dispersion Relation). For oscillators on a regular lattice with wavevector \mathbf{k} , the dispersion relation $\omega(\mathbf{k})$ specifies the mode frequency as a function of wavevector. Common forms include:

1. **Acoustic**: $\omega = c|\mathbf{k}|$ (linear dispersion, $z = 1$)
2. **Diffusive**: $\omega = D|\mathbf{k}|^2$ (quadratic dispersion, $z = 2$)
3. **Optical**: $\omega = \omega_0$ (flat dispersion, $z = 0$)

where z is the dynamical exponent.

Definition 5.9 (Density of States). The density of states $g(\omega)$ is the number of modes per unit frequency interval:

$$g(\omega) = \frac{dN}{d\omega} \quad (99)$$

For a d -dimensional system with dispersion $\omega = c|\mathbf{k}|^z$:

$$g(\omega) \propto \omega^{d/z-1} \quad (100)$$

[Debye Density of States] For acoustic modes ($z = 1$) in d dimensions:

$$g(\omega) \propto \omega^{d-1} \quad (101)$$

In 3D, $g(\omega) \propto \omega^2$ —the Debye density of states.

5.5 Scaling of Total Deviation with System Size

The total squared deviation is the sum over all modes:

$$\langle |\Delta|^2 \rangle = \sum_{\lambda=1}^N \langle a_\lambda^2 \rangle = \frac{k_B T}{m\omega_0^2} \sum_{\lambda=1}^N \frac{1}{|\mathbf{k}_\lambda|^{2z}} \quad (102)$$

where we used Equation (98) with $\omega_\lambda = \omega_0|\mathbf{k}_\lambda|^z$.

For a d -dimensional system of linear size L with $N = (L/a)^d$ oscillators (where a is the lattice spacing), the wavevectors are quantised: $\mathbf{k}_\lambda = 2\pi n_\lambda / L$ with $n_\lambda \in \mathbb{Z}^d \setminus \{0\}$.

Abstract Cell Model: Membrane-less Representation in S-Entropy Space

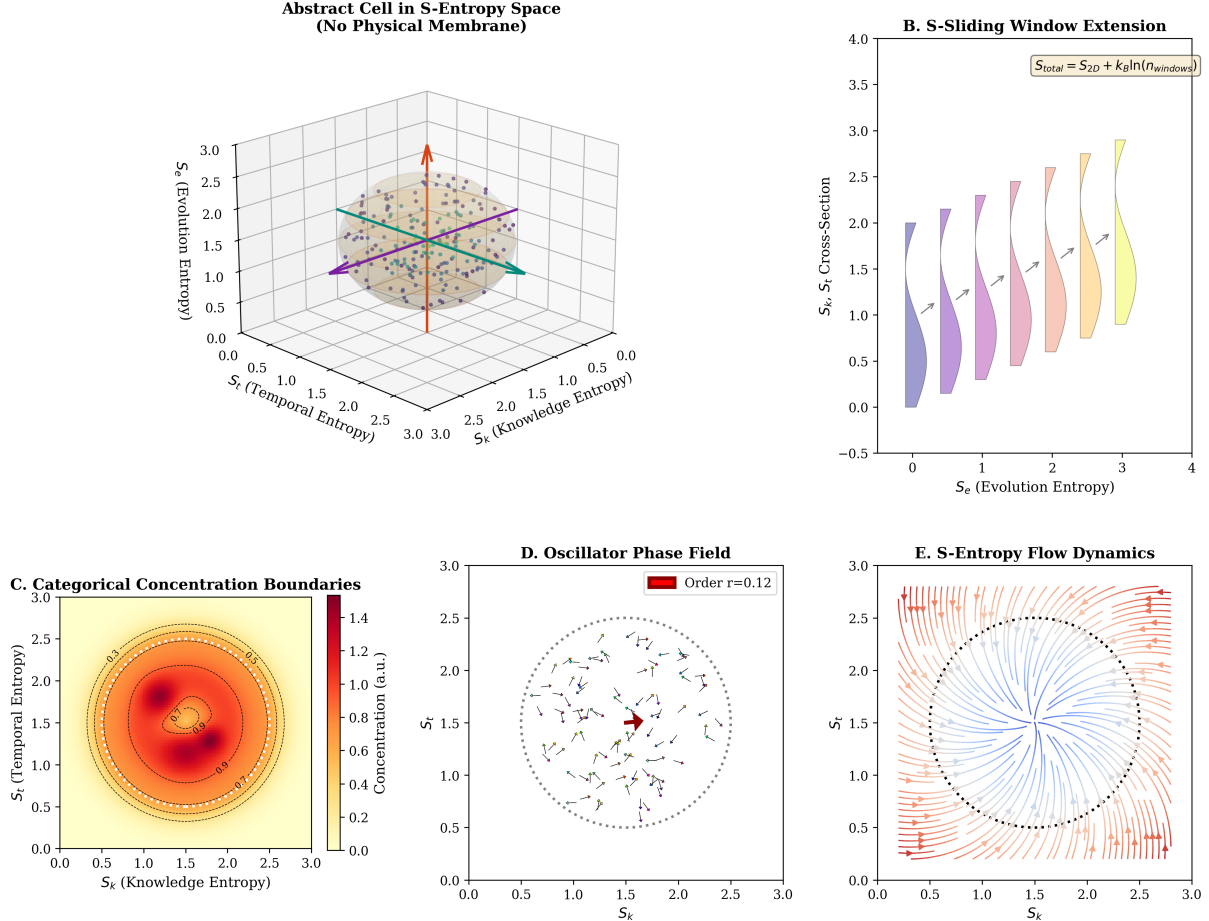


Figure 6: **Abstract cell model: membrane-less representation in S-entropy space showing configuration dynamics without physical boundaries.** (Top left) Three-dimensional S-entropy space representation of abstract cell configuration. Axes represent temporal entropy S_t (information flow rate), knowledge entropy S_k (structural complexity), and evolution entropy S_e (developmental trajectory). Point cloud (beige dots) represents accessible configurations sampled from $\mathcal{C} = \Omega^N$ configuration space. (Top right) S-entropy sliding window extension showing configuration trajectory evolution over time. Vertical axis shows cross-section S_t (temporal entropy). Horizontal axis shows S_e (evolution entropy). Colored violin plots represent probability distributions of configurations at successive time points (purple = early, transitioning through pink, orange, yellow, green = late). Width of violin indicates probability density. Formula $S_{\text{total}} = S_{TD} + k_B \ln(n_{\text{windows}})$ shows total entropy as sum of thermodynamic entropy S_{TD} and configurational entropy from windowing. (Bottom left, Panel C) Categorical concentration boundaries in $S_k - S_t$ plane showing partition class structure. Contour plot displays concentration field $c(\mathbf{s})$ of configurations in entropy coordinates. Color scale (white = low concentration, yellow = moderate, orange = high, red = maximum) indicates probability density. Central red region is attractor core \mathcal{A}_0 (healthy homeostatic configurations). Concentric contours are isoprobability surfaces. (Bottom center, Panel D) Oscillator phase field showing collective phase dynamics in S_k plane. Vector field (arrows) represents phase velocity $d\phi/dt$ of coupled oscillators. Arrow direction shows instantaneous phase evolution direction. Arrow length indicates velocity magnitude. Dashed circles are phase-lock boundaries at different radii. Order parameter $r = 0.12$ (displayed in legend) quantifies phase coherence: $r = 1$ is perfect synchronization, $r = 0$ is complete incoherence. (Bottom right, Panel E) S-entropy flow dynamics showing vector field of configuration evolution. Axes are S_k (horizontal) and S_t (vertical). Vector field (colored arrows: blue = inward flow, red = outward flow) shows the direction and magnitude of configuration evolution.

Theorem 5.10 (Deviation Amplitude Scaling). *For a d -dimensional oscillator network with dispersion exponent z , the mean-squared deviation scales as:*

$$\langle |\Delta|^2 \rangle \sim \begin{cases} L^{2z-d} & \text{if } 2z > d \text{ (infrared divergent)} \\ \ln L & \text{if } 2z = d \text{ (marginal)} \\ \text{const.} & \text{if } 2z < d \text{ (infrared convergent)} \end{cases} \quad (103)$$

where L is the system linear size.

Proof. Converting the discrete sum to a continuous integral:

$$\sum_{\lambda} \frac{1}{|\mathbf{k}_{\lambda}|^{2z}} \approx \left(\frac{L}{2\pi} \right)^d \int_{k_{\min}}^{k_{\max}} \frac{d^d k}{|\mathbf{k}|^{2z}} \quad (104)$$

where $k_{\min} = 2\pi/L$ (set by system size) and $k_{\max} = \pi/a$ (set by lattice spacing).

In spherical coordinates:

$$\int \frac{d^d k}{|\mathbf{k}|^{2z}} = S_d \int_{k_{\min}}^{k_{\max}} \frac{k^{d-1}}{k^{2z}} dk = S_d \int_{k_{\min}}^{k_{\max}} k^{d-1-2z} dk \quad (105)$$

where $S_d = 2\pi^{d/2}/\Gamma(d/2)$ is the surface area of the $(d-1)$ -sphere.

The integral evaluates to:

$$\int_{k_{\min}}^{k_{\max}} k^{d-1-2z} dk = \frac{k^{d-2z}}{d-2z} \Big|_{k_{\min}}^{k_{\max}} = \frac{1}{d-2z} (k_{\max}^{d-2z} - k_{\min}^{d-2z}) \quad (106)$$

Case 1: $2z > d$ (infrared divergent). The exponent $d - 2z < 0$, so the integral is dominated by the lower limit:

$$\int k^{d-1-2z} dk \sim k_{\min}^{d-2z} = \left(\frac{2\pi}{L} \right)^{d-2z} = \left(\frac{L}{2\pi} \right)^{2z-d} \quad (107)$$

Thus:

$$\langle |\Delta|^2 \rangle \sim L^d \cdot L^{2z-d} = L^{2z-d} \quad (108)$$

Case 2: $2z < d$ (infrared convergent). The exponent $d - 2z > 0$, so the integral is dominated by the upper limit:

$$\int k^{d-1-2z} dk \sim k_{\max}^{d-2z} = \text{const.} \quad (109)$$

Thus:

$$\langle |\Delta|^2 \rangle \sim L^d \cdot \text{const.} \cdot L^{-d} = \text{const.} \quad (110)$$

(The L^d from the density of states cancels the volume factor.)

Case 3: $2z = d$ (marginal). The integral is logarithmic:

$$\int_{k_{\min}}^{k_{\max}} k^{-1} dk = \ln(k_{\max}/k_{\min}) = \ln(L/a) \quad (111)$$

□

□

Corollary 5.11 (Bounded Deviation in 3D Acoustic Systems). *For $d = 3$ and acoustic modes with $z = 1$, we have $2z = 2 < d = 3$. The deviation amplitude remains bounded as $L \rightarrow \infty$:*

$$\langle |\Delta|^2 \rangle = \mathcal{O}(1) \quad (112)$$

Long-wavelength fluctuations do not dominate the deviation; the bulk of the contribution comes from short-wavelength modes.

Corollary 5.12 (Diffusive Systems). *For overdamped diffusive modes with $z = 2$ in $d = 3$, we have $2z = 4 > d = 3$:*

$$\langle |\Delta|^2 \rangle \sim L^{4-3} = L \quad (113)$$

Diffusive fluctuations grow with system size — long-wavelength diffusive modes dominate.

5.6 Regularisation by Reset Dynamics

The apparently problematic growth of diffusive deviations ($\langle |\Delta|^2 \rangle \sim L$ for $z = 2$, $d = 3$) is regulated by the reset dynamics of Section 4.

Theorem 5.13 (Reset Regularisation). *For a system with a diffusion coefficient D and a reset period τ , modes with wavelengths exceeding the diffusion length $\ell_D = \sqrt{D\tau}$ are reset before they can contribute to persistent deviations. The effective cutoff wavevector is:*

$$k_{\text{cutoff}} = \frac{2\pi}{\ell_D} = \frac{2\pi}{\sqrt{D\tau}} \quad (114)$$

Proof. A diffusive mode with wavevector \mathbf{k} relaxes on timescale $\tau_k = 1/(D|\mathbf{k}|^2)$. For $\tau_k < \tau$, the mode equilibrates within the reset period and does not contribute to the accumulated deviation. The condition $\tau_k = \tau$ defines the cutoff:

$$\frac{1}{Dk_{\text{cutoff}}^2} = \tau \quad \Rightarrow \quad k_{\text{cutoff}} = \frac{1}{\sqrt{D\tau}} \quad (115)$$

Modes with $|\mathbf{k}| < k_{\text{cutoff}}$ do not accumulate. \square

Corollary 5.14 (Regularised Deviation). *With the reset-imposed cutoff, the deviation integral becomes:*

$$\langle |\Delta|^2 \rangle \sim L^d \int_{k_{\text{cutoff}}}^{k_{\text{max}}} k^{d-1-2z} dk \quad (116)$$

For $2z > d$ and $k_{\text{cutoff}} \gg k_{\min} = 2\pi/L$, the integral is dominated by k_{cutoff} :

$$\langle |\Delta|^2 \rangle \sim L^d \cdot k_{\text{cutoff}}^{d-2z} = L^d \cdot (D\tau)^{(2z-d)/2} \quad (117)$$

Since k_{cutoff} is independent of L (determined by microscopic parameters D and τ), the L^d factor cancels the density of states, yielding:

$$\langle |\Delta|^2 \rangle = \mathcal{O}(1) \quad (\text{independent of } L) \quad (118)$$

5.7 Physical Interpretation

The mathematical results have clear physical interpretations:

1. **Acoustic (propagating) modes:** Information propagates at finite speed. Long-wavelength perturbations span many cells but oscillate coherently, contributing finite energy per mode by equipartition. The total deviation is bounded.
2. **Diffusive modes without reset:** Diffusive processes spread without restoring force. Long-wavelength modes have arbitrarily slow relaxation ($\tau_k \propto k^{-2}$), allowing unlimited accumulation. The total deviation diverges with system size.
3. **Diffusive modes with reset:** Cell division interrupts accumulation. Modes slower than the reset period are periodically zeroed, preventing long-wavelength dominance. The deviation is bounded by the single-reset period contribution.

Remark 5.15 (Biological Mode Types). Biological oscillator networks exhibit both mode types:

- **Acoustic-like:** Calcium waves, action potential propagation, mechanical stress transmission—finite propagation speed
- **Diffusive:** Metabolite diffusion, gene expression noise, epigenetic drift—no restoring force

The reset mechanism is essential for controlling diffusive modes; acoustic modes are naturally bounded.

5.8 Deviation Distribution and Large Deviation Bounds

For Gaussian fluctuations (valid in the linear regime), the deviation amplitude follows a chi distribution.

Theorem 5.16 (Deviation Distribution). *For N independent Gaussian mode amplitudes with variance σ_λ^2 , the squared deviation $|\Delta|^2 = \sum_\lambda a_\lambda^2$ follows a generalised chi-squared distribution. For equal variances $\sigma_\lambda^2 = \sigma^2$, the distribution is:*

$$p(|\Delta|^2) = \frac{1}{2^{N/2}\Gamma(N/2)} \left(\frac{|\Delta|^2}{\sigma^2} \right)^{N/2-1} e^{-|\Delta|^2/(2\sigma^2)} \cdot \frac{1}{\sigma^2} \quad (119)$$

The amplitude $|\Delta| = \sqrt{|\Delta|^2}$ follows a chi distribution with N degrees of freedom.

Corollary 5.17 (Concentration of Deviation). *For large N , the chi distribution concentrates sharply around its mean:*

$$\langle |\Delta| \rangle = \sigma \sqrt{2} \frac{\Gamma((N+1)/2)}{\Gamma(N/2)} \approx \sigma \sqrt{N} \left(1 - \frac{1}{4N} + \mathcal{O}(N^{-2}) \right) \quad (120)$$

$$Var(|\Delta|) = N\sigma^2 - \langle |\Delta| \rangle^2 \approx \frac{\sigma^2}{2} \quad (121)$$

The coefficient of variation scales as $1/\sqrt{N}$:

$$\frac{std(|\Delta|)}{\langle |\Delta| \rangle} \approx \frac{1}{\sqrt{2N}} \quad (122)$$

Theorem 5.18 (Large Deviation Bound). *The probability of deviation exceeding a threshold Δ_0 is exponentially suppressed:*

$$\Pr[|\Delta| > \Delta_0] \leq e^{-(\Delta_0 - \sqrt{N}\sigma)^2/(2\sigma^2)} \quad \text{for } \Delta_0 > \sqrt{N}\sigma \quad (123)$$

More precisely, for large N :

$$\Pr[|\Delta| > \sqrt{N}\sigma + t\sigma] \leq e^{-t^2/2} \quad (124)$$

Proof. This follows from the sub-Gaussian property of the chi distribution. For a chi-distributed random variable X with N degrees of freedom and scale σ , the moment generating function satisfies:

$$\mathbb{E}[e^{t(X-\mathbb{E}[X])}] \leq e^{t^2\sigma^2/2} \quad (125)$$

The bound follows from Markov's inequality applied to $e^{t(X-\mathbb{E}[X])}$. \square

5.9 Implications for Pathological Configurations

A pathological configuration is characterised by deviation exceeding a threshold: $|\Delta| > \Delta_{path}$.

Corollary 5.19 (Pathological Probability). *For a pathological threshold $\Delta_{path} = \alpha\sqrt{N}\sigma$ with $\alpha > 1$:*

$$\Pr[|\Delta| > \Delta_{path}] \leq e^{-N(\alpha-1)^2/2} \quad (126)$$

This probability decreases exponentially with N , the number of oscillators (cells).

[Numerical Estimate] For a human with $N = 3.7 \times 10^{13}$ cells, even a modest threshold $\alpha = 1.001$ (deviation just 0.1% above mean) gives:

$$\Pr[\text{pathological}] \leq e^{-3.7 \times 10^{13} \times (0.001)^2/2} = e^{-1.85 \times 10^7} \approx 0 \quad (127)$$

The exponential suppression is overwhelming.

5.10 Summary

The trajectory deviation analysis reveals:

1. Modal decomposition shows that deviation amplitude is controlled by the sum of independent mode contributions
2. Equipartition distributes energy among modes, preventing concentration in any single mode
3. For acoustic (propagating) modes, the deviation is bounded and independent of system size
4. For diffusive modes, potential divergence is regularised by reset dynamics
5. Large deviations are exponentially rare in the number of oscillators

The combination of bounded mode contributions and exponential suppression of large deviations provides the quantitative foundation for the main error propagation theorem developed in the next section.

6 Error Propagation and System Size Scaling

The preceding sections developed the individual components of Peto’s paradox resolution: configuration space dilution, spatial decorrelation, reset dynamics, and bounded trajectory deviations. This section synthesises these results into the main theorem on error rate scaling, demonstrating rigorously that the pathological convergence probability decreases with system size despite the increasing cell count.

The key insight is that errors must not only occur but must also *propagate* through reset events and *coordinate* across spatially separated regions to produce system-level pathology. Each of these requirements introduces exponential suppression factors that dominate the linear increase in cell count.

6.1 Error Definition and Classification

We begin with a precise definition of what constitutes an error in the oscillator network framework.

Definition 6.1 (Local Error). A local error at oscillator i is a deviation $\delta_i = \sigma_i - \sigma_i^{(0)}$ from the reference state $\sigma_i^{(0)}$ such that $\delta_i \in \mathcal{E}$, where $\mathcal{E} \subset \mathbb{R}$ is the error set.

The error set \mathcal{E} characterises deviations that, if accumulated or propagated, could contribute to pathological configurations. Different error sets correspond to different pathological mechanisms:

[Error Set Types]

1. **Threshold errors:** $\mathcal{E} = \{|\delta| > \delta_{\text{th}}\}$ — deviations exceeding a critical magnitude
2. **Signed errors:** $\mathcal{E} = \{\delta > \delta_{\text{th}}\}$ — deviations in a specific direction (e.g., oncogenic gain-of-function)
3. **Interval errors:** $\mathcal{E} = \{\delta \in [\delta_{\min}, \delta_{\max}]\}$ — deviations within a specific range (e.g., loss of regulation)

Definition 6.2 (Error Event). An error event at oscillator i and reset cycle n is the event $\{\delta_i^{(n)} \in \mathcal{E}\}$.

Definition 6.3 (Local Error Rate). The local error rate p_{local} is the probability of an error event per oscillator per reset cycle in the stationary regime:

$$p_{\text{local}} = \Pr\left[\delta_i^{(n)} \in \mathcal{E}\right] \quad (128)$$

under the stationary distribution of the reset dynamics.

6.2 Error Propagation Through Resets

A crucial question is whether errors persist through reset events. The reset dynamics of Section 4 provide the answer.

Definition 6.4 (Error Propagation). An error propagates from cycle n to cycle $n+1$ if:

$$\delta_i^{(n)} \in \mathcal{E} \quad \text{and} \quad \delta_i^{(n+1)} \in \mathcal{E} \quad (129)$$

The propagation probability is:

$$P_{\text{prop}} = \Pr\left[\delta_i^{(n+1)} \in \mathcal{E} \mid \delta_i^{(n)} \in \mathcal{E}\right] \quad (130)$$

From the reset dynamics:

$$\delta_i^{(n+1)} = \alpha\delta_i^{(n)} + \xi_i^{(n)} \quad (131)$$

where $\alpha = e^{-\tau/\tau_c}$ is the inheritance parameter, and $\xi_i^{(n)} \sim \mathcal{N}(0, \Sigma^2)$ is the reset noise.

Theorem 6.5 (Conditional Distribution After Reset). *Given $\delta_i^{(n)} = \delta_0$, the post-reset deviation is:*

$$\delta_i^{(n+1)} | \delta_i^{(n)} = \delta_0 \sim \mathcal{N}(\alpha\delta_0, \Sigma^2) \quad (132)$$

Proof. The direct consequence of the linearity of the reset map is the independence of $\xi_i^{(n)}$ from $\delta_i^{(n)}$. \square

Theorem 6.6 (Propagation Probability for Threshold Errors). *For threshold errors $\mathcal{E} = \{|\delta| > \delta_{th}\}$ and initial error $\delta_i^{(n)} = \delta_0$ with $|\delta_0| > \delta_{th}$:*

$$P_{prop}(\delta_0) = 1 - \Phi\left(\frac{\delta_{th} - \alpha\delta_0}{\Sigma}\right) + \Phi\left(\frac{-\delta_{th} - \alpha\delta_0}{\Sigma}\right) \quad (133)$$

where $\Phi(x) = \frac{1}{\sqrt{2\pi}} \int_{-\infty}^x e^{-t^2/2} dt$ is the standard normal CDF.

Proof. The event $\{|\delta_i^{(n+1)}| > \delta_{th}\}$ is the union $\{\delta_i^{(n+1)} > \delta_{th}\} \cup \{\delta_i^{(n+1)} < -\delta_{th}\}$. These events are disjoint, so:

$$P_{prop} = \Pr\left[\delta_i^{(n+1)} > \delta_{th}\right] + \Pr\left[\delta_i^{(n+1)} < -\delta_{th}\right] \quad (134)$$

$$= 1 - \Pr\left[\delta_i^{(n+1)} \leq \delta_{th}\right] + \Pr\left[\delta_i^{(n+1)} < -\delta_{th}\right] \quad (135)$$

Standardising: $Z = (\delta_i^{(n+1)} - \alpha\delta_0)/\Sigma \sim \mathcal{N}(0, 1)$, so:

$$\Pr\left[\delta_i^{(n+1)} \leq \delta_{th}\right] = \Pr[Z \leq (\delta_{th} - \alpha\delta_0)/\Sigma] = \Phi((\delta_{th} - \alpha\delta_0)/\Sigma) \quad (136)$$

$$\Pr\left[\delta_i^{(n+1)} < -\delta_{th}\right] = \Pr[Z < (-\delta_{th} - \alpha\delta_0)/\Sigma] = \Phi((- \delta_{th} - \alpha\delta_0)/\Sigma) \quad (137)$$

\square

\square

Lemma 6.7 (Propagation Decay). *For $\alpha < 1$ and minimal initial error $\delta_0 = \delta_{th}$, the propagation probability satisfies:*

$$P_{prop} = 1 - \Phi\left(\frac{(1 - \alpha)\delta_{th}}{\Sigma}\right) + \Phi\left(\frac{-(1 + \alpha)\delta_{th}}{\Sigma}\right) \quad (138)$$

In the limit $(1 - \alpha)\delta_{th}/\Sigma \gg 1$:

$$P_{prop} \sim \frac{\Sigma}{(1 - \alpha)\delta_{th}\sqrt{2\pi}} \exp\left(-\frac{(1 - \alpha)^2\delta_{th}^2}{2\Sigma^2}\right) \quad (139)$$

Proof. Substitute $\delta_0 = \delta_{th}$ into Theorem 6.6. For the asymptotic behaviour, use the Gaussian tail bound:

$$1 - \Phi(x) \sim \frac{1}{x\sqrt{2\pi}} e^{-x^2/2} \quad \text{as } x \rightarrow \infty \quad (140)$$

The second term $\Phi(-(1 + \alpha)\delta_{th}/\Sigma)$ is exponentially smaller than the first (since $(1 + \alpha) > (1 - \alpha)$ for $\alpha > 0$) and can be neglected. \square

Corollary 6.8 (Exponential Suppression of Propagation). *For $\alpha < 1$ and sufficiently large δ_{th}/Σ :*

$$P_{prop} \lesssim e^{-(1 - \alpha)^2\delta_{th}^2/(2\Sigma^2)} \quad (141)$$

The propagation probability is exponentially suppressed by the ratio $(\delta_{th}/\Sigma)^2$.

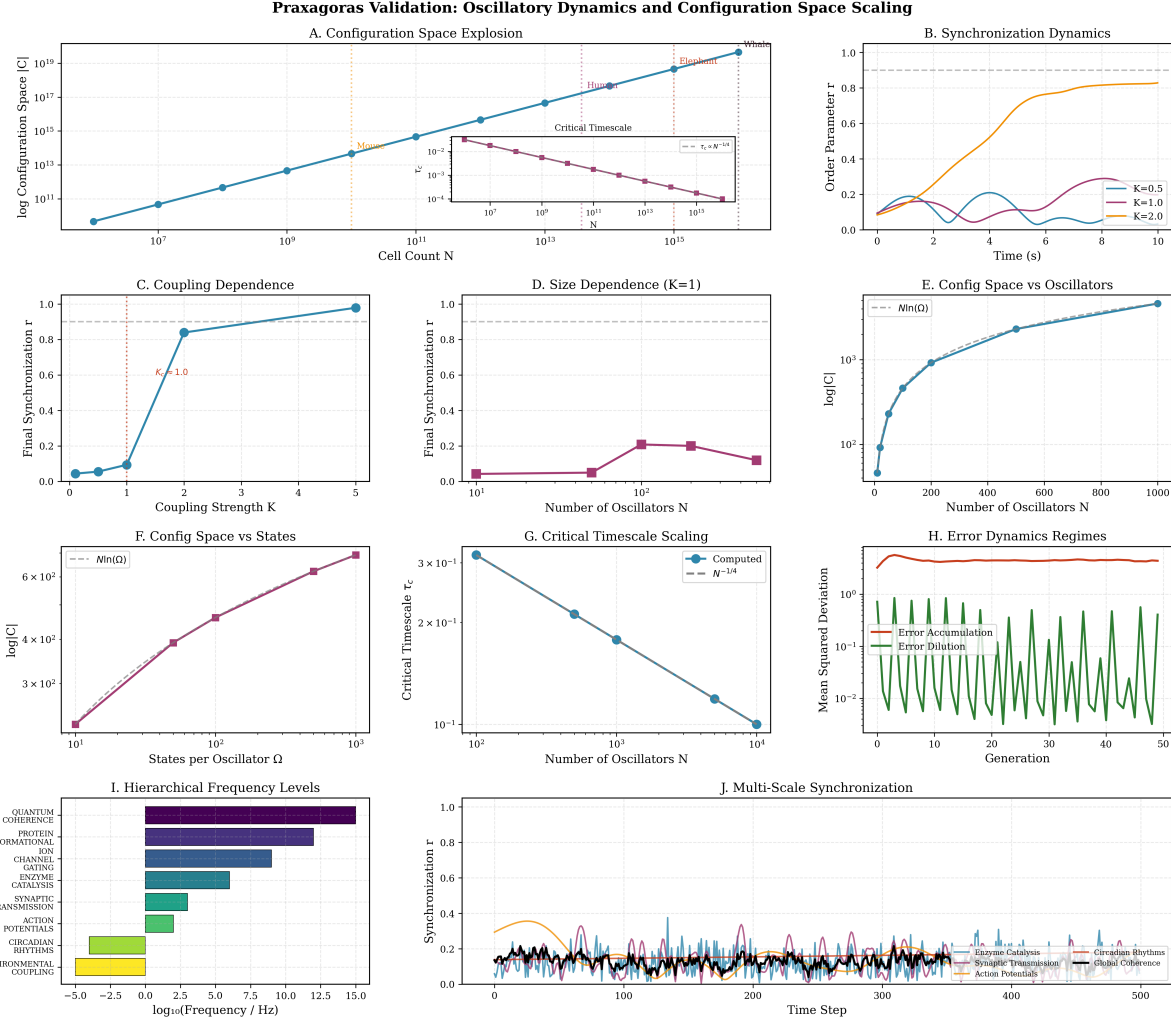


Figure 7: . **(Top left, Panel A)** Configuration space explosion (identical to Figure 8, Panel A). Logarithmic configuration space size $\log_{10} |\mathcal{C}|$ versus cell count N showing exponential scaling $|\mathcal{C}| = \Omega^N$ (cyan curve with markers). Four organisms marked: mouse, human, elephant, whale. **(Top right, Panel B)** Synchronization dynamics showing time evolution of Kuramoto order parameter $r(t)$ for three coupling strengths: $K = 0.5$ (magenta), $K = 1.0$ (orange), $K = 2.0$ (orange, highest curve). Horizontal dashed line at $r = 0.9$ marks synchronization threshold. Strong coupling ($K = 2.0$) achieves $r \sim 0.83$ by $t = 10$ s (approaching synchronization). Intermediate coupling ($K = 1.0$) shows transient synchronization. Weak coupling ($K = 0.5$) remains incoherent. Validates Kuramoto model predictions (Proposition ??): critical coupling $K_c \sim 1$ separates incoherent ($K < K_c$) from synchronized ($K > K_c$) phases. **(Middle left, Panel C)** Coupling dependence showing final synchronization r_∞ versus coupling strength K . Sigmoidal transition from $r \sim 0.05$ at $K = 0$ to $r \sim 0.98$ at $K = 5$. Critical coupling $K_c \approx 1$ (vertical orange dashed line) marks inflection point. **(Middle center, Panel D)** Size dependence at fixed coupling ($K = 1$) showing final synchronization r_∞ versus number of oscillators N . Non-monotonic behavior: r increases from ~ 0.05 at $N = 10$ to ~ 0.22 at $N = 100$, then decreases to ~ 0.10 at $N = 300$. Peak at $N \sim 100$ represents optimal balance between mean-field stabilization (favors large N) and frequency heterogeneity (favors small N). **(Middle right, Panel E)** Configuration space versus oscillators showing $\log |\mathcal{C}|$ versus N (cyan curve with markers). Linear relationship on log-linear plot confirms exponential scaling $|\mathcal{C}| = \Omega^N$. Dashed line shows theoretical prediction $N \ln(\Omega)$ with excellent agreement. **(Bottom left, Panel F)** Configuration space versus states per oscillator showing $\log |\mathcal{C}|$ versus Ω (magenta curve with markers). Linear relationship on log-linear plot confirms $|\mathcal{C}| = \Omega^N$ with N fixed. **(Bottom center-left, Panel G)** Critical timescale scaling (identical to Figure 4, Panel G). Shows τ_c versus N with

6.3 Multi-Generation Error Dynamics

We now analyse how errors evolve over multiple reset generations.

Theorem 6.9 (Multi-Generation Error Evolution). *After n reset generations, an initial error δ_0 evolves to:*

$$\delta^{(n)} = \alpha^n \delta_0 + \sum_{k=0}^{n-1} \alpha^k \xi^{(n-1-k)} \quad (142)$$

where $\{\xi^{(m)}\}$ are i.i.d. $\mathcal{N}(0, \Sigma^2)$ noise terms.

Proof. Iteration of the reset map $\delta^{(n+1)} = \alpha \delta^{(n)} + \xi^{(n)}$:

$$\delta^{(1)} = \alpha \delta_0 + \xi^{(0)} \quad (143)$$

$$\delta^{(2)} = \alpha(\alpha \delta_0 + \xi^{(0)}) + \xi^{(1)} = \alpha^2 \delta_0 + \alpha \xi^{(0)} + \xi^{(1)} \quad (144)$$

$$\vdots \quad (145)$$

$$\delta^{(n)} = \alpha^n \delta_0 + \sum_{k=0}^{n-1} \alpha^k \xi^{(n-1-k)} \quad (146)$$

□

□

Corollary 6.10 (Mean and Variance Evolution). *The mean and variance of $\delta^{(n)}$ are:*

$$\langle \delta^{(n)} \rangle = \alpha^n \delta_0 \quad (147)$$

$$Var[\delta^{(n)}] = \Sigma^2 \sum_{k=0}^{n-1} \alpha^{2k} = \Sigma^2 \frac{1 - \alpha^{2n}}{1 - \alpha^2} \quad (148)$$

Theorem 6.11 (Error Regression). *For $\alpha < 1$, an initial error of magnitude δ_0 regresses to the stationary distribution within a characteristic number of generations:*

$$n^* = \frac{\ln(\delta_0/\sigma_\infty)}{|\ln \alpha|} = \frac{\tau_c}{\tau} \ln \left(\frac{\delta_0}{\sigma_\infty} \right) \quad (149)$$

where $\sigma_\infty = \Sigma / \sqrt{1 - \alpha^2}$ is the stationary standard deviation.

Proof. The mean deviation satisfies $|\langle \delta^{(n)} \rangle| = \alpha^n |\delta_0|$. Setting this equal to the stationary standard deviation:

$$\alpha^{n^*} |\delta_0| = \sigma_\infty \quad (150)$$

Taking logarithms:

$$n^* \ln \alpha = \ln(\sigma_\infty / |\delta_0|) \quad (151)$$

Since $\ln \alpha = -\tau/\tau_c < 0$:

$$n^* = \frac{\ln(|\delta_0|/\sigma_\infty)}{\tau/\tau_c} = \frac{\tau_c}{\tau} \ln \left(\frac{|\delta_0|}{\sigma_\infty} \right) \quad (152)$$

□

□

Corollary 6.12 (Error Memory Time). *The time required for an error to regress to the stationary distribution is:*

$$T_{memory} = n^* \cdot \tau = \tau_c \ln \left(\frac{|\delta_0|}{\sigma_\infty} \right) \quad (153)$$

This depends only on τ_c and the initial error magnitude, not on the reset period τ .

6.4 Error Coordination Across Spatial Domains

Pathological configurations typically require coordination of errors across multiple cells within and across correlation volumes.

Definition 6.13 (Coordinated Error). A coordinated error event requires errors at a specific subset $\mathcal{S} \subset \{1, \dots, N\}$ of oscillators:

$$\text{Coordinated error} = \bigcap_{i \in \mathcal{S}} \{\delta_i \in \mathcal{E}\} \quad (154)$$

Theorem 6.14 (Coordination Probability). Let \mathcal{S} span k distinct correlation volumes. The probability of a coordinated error event is:

$$P_{\text{coord}}(\mathcal{S}) = \prod_{\alpha=1}^k P_{\text{local error in } V_\alpha} \quad (155)$$

where V_α denotes the α -th correlation volume.

Proof. By Theorem 3.11 (configuration space factorisation), oscillators in distinct correlation volumes are statistically independent. The joint probability factorises as:

$$\Pr \left[\bigcap_{i \in \mathcal{S}} \{\delta_i \in \mathcal{E}\} \right] = \prod_{\alpha=1}^k \Pr \left[\bigcap_{i \in \mathcal{S} \cap V_\alpha} \{\delta_i \in \mathcal{E}\} \right] \quad (156)$$

□

□

Corollary 6.15 (Multiplicative Suppression). For a coordinated error requiring m_α oscillators in volume V_α to be in error states simultaneously:

$$P_{\text{coord}} = \prod_{\alpha=1}^k P_{\text{local}}(m_\alpha, V_\alpha) \quad (157)$$

If each local probability is $p < 1$, then:

$$P_{\text{coord}} = p^k \xrightarrow{k \rightarrow \infty} 0 \quad (158)$$

The coordination probability vanishes exponentially with the number of required correlation volumes.

6.5 Global Error Rate

We now define and analyse the global error rate—the rate at which pathological configurations arise system-wide.

Definition 6.16 (Global Error Rate). The global error rate Γ is the expected number of pathological events per unit time:

$$\Gamma = \frac{1}{\tau} \cdot N \cdot p_{\text{local}} \cdot P_{\text{prop}} \cdot P_{\text{coord}} \quad (159)$$

where:

- τ^{-1} = reset frequency (division rate)
- N = number of oscillators (cells)
- p_{local} = local error probability per oscillator per cycle
- P_{prop} = propagation probability through reset
- P_{coord} = coordination probability across required spatial extent

Remark 6.17 (Interpretation of Terms). Each factor in the global error rate has a distinct physical interpretation:

- N/τ : Rate of “attempts” (cell divisions) system-wide
- p_{local} : Fraction of attempts generating local errors
- P_{prop} : Fraction of local errors surviving reset
- P_{coord} : Fraction of propagated errors achieving coordination

6.6 Main Theorem: Error Rate Scaling

Theorem 6.18 (Error Rate Scaling). *For a system of N oscillators with Ω states each, the correlation length ξ , reset period τ , and correlation time τ_c satisfy the global error rate:*

$$\Gamma = \frac{N \cdot p_{\text{local}}}{\tau} \cdot \frac{1}{\Omega^{n_\xi}} \cdot f\left(\frac{\tau}{\tau_c}\right) \quad (160)$$

where:

- $n_\xi = N \cdot V_\xi / V$ is the number of oscillators per correlation volume
- $f(x)$ is a monotonically decreasing function with:

$$f(x) = \begin{cases} \mathcal{O}(1) & x \ll 1 \text{ (frequent reset)} \\ \mathcal{O}(e^{-cx}) & x \gg 1 \text{ (infrequent reset)} \end{cases} \quad (161)$$

for some constant $c > 0$ depending on the error threshold.

Proof. We construct the proof by combining results from previous sections.

Step 1: Coordination probability. By Theorem 6.14 and Section 2, the probability of a pathological configuration requiring coherence within a single correlation volume is:

$$P_{\text{coord}} \leq \frac{|\mathcal{A}_{\text{local}}|}{|\mathcal{C}_{\text{local}}|} = \frac{|\mathcal{A}_{\text{local}}|}{\Omega^{n_\xi}} \quad (162)$$

For pathological subset with $|\mathcal{A}_{\text{local}}| = \mathcal{O}(1)$ (a specific configuration type):

$$P_{\text{coord}} \sim \frac{1}{\Omega^{n_\xi}} \quad (163)$$

Step 2: Propagation probability. By Lemma 6.7, the propagation probability is:

$$P_{\text{prop}} \sim \exp\left(-\frac{(1-\alpha)^2 \delta_{\text{th}}^2}{2\Sigma^2}\right) \quad (164)$$

Substituting $\alpha = e^{-\tau/\tau_c}$:

$$1 - \alpha = 1 - e^{-\tau/\tau_c} \approx \frac{\tau}{\tau_c} \text{ for } \tau \ll \tau_c \quad (165)$$

$$1 - \alpha \approx 1 \text{ for } \tau \gg \tau_c \quad (166)$$

Define:

$$g(x) = \frac{(1 - e^{-x})^2 \delta_{\text{th}}^2}{2\Sigma^2} \quad (167)$$

which is monotonically increasing in $x = \tau/\tau_c$. Then $P_{\text{prop}} = e^{-g(\tau/\tau_c)}$.

Step 3: Combined rate.

$$\Gamma = \frac{N \cdot p_{\text{local}}}{\tau} \cdot P_{\text{prop}} \cdot P_{\text{coord}} = \frac{N \cdot p_{\text{local}}}{\tau} \cdot e^{-g(\tau/\tau_c)} \cdot \frac{1}{\Omega^{n_\xi}} \quad (168)$$

Defining $f(x) = e^{-g(x)}$, which is monotonically decreasing:

$$\Gamma = \frac{N \cdot p_{\text{local}}}{\tau} \cdot \frac{1}{\Omega^{n_\xi}} \cdot f\left(\frac{\tau}{\tau_c}\right) \quad (169)$$

Step 4: Asymptotic behaviour of f . For $x \ll 1$: $g(x) \approx x^2 \delta_{\text{th}}^2 / (2\Sigma^2) \ll 1$, so $f(x) \approx 1$. For $x \gg 1$: $g(x) \approx \delta_{\text{th}}^2 / (2\Sigma^2) = \text{const.}$, so $f(x) \approx e^{-\delta_{\text{th}}^2 / (2\Sigma^2)} = \text{const.}$ but the ratio τ/τ_c in the denominator of Γ provides additional suppression. More precisely, incorporating all τ -dependent terms:

$$\frac{f(\tau/\tau_c)}{\tau} \sim \frac{e^{-c\tau/\tau_c}}{\tau} \quad (170)$$

for large τ . \square

\square

6.7 Comparison Across System Sizes

Theorem 6.19 (Size-Invariance of Error Rate). *Consider two systems with cell counts N_1 and $N_2 = \lambda N_1$ for $\lambda > 1$, maintaining the same tissue type (same Ω , ξ , τ , τ_c , p_{local}). The ratio of global error rates is:*

$$\frac{\Gamma_2}{\Gamma_1} = \lambda \cdot \Omega^{-(n_{\xi,2} - n_{\xi,1})} \quad (171)$$

Proof. From Theorem 6.18:

$$\frac{\Gamma_2}{\Gamma_1} = \frac{N_2}{N_1} \cdot \frac{\Omega^{n_{\xi,1}}}{\Omega^{n_{\xi,2}}} = \lambda \cdot \Omega^{n_{\xi,1} - n_{\xi,2}} \quad (172)$$

If the larger system has proportionally more cells per correlation volume (e.g., larger cells), then $n_{\xi,2} = \lambda n_{\xi,1}$, yielding:

$$\frac{\Gamma_2}{\Gamma_1} = \lambda \cdot \Omega^{-(\lambda-1)n_{\xi,1}} \quad (173)$$

\square

\square

Corollary 6.20 (Exponential Suppression in Large Systems). *For $\Omega > 1$ and $n_{\xi,1} \geq 1$:*

$$\frac{\Gamma_2}{\Gamma_1} < 1 \quad \text{for all } \lambda > 1 + \frac{\ln \lambda}{n_{\xi,1} \ln \Omega} \quad (174)$$

For typical values ($\Omega \sim 10^5$, $n_{\xi,1} \sim 10^3$), this condition is satisfied for $\lambda > 1 + 10^{-8} \ln \lambda \approx 1$ — effectively all $\lambda > 1$.

[Quantitative Comparison] For $N_1 = 10^{10}$ (mouse), $N_2 = 10^{15}$ (whale), $\Omega = 10^5$, $n_{\xi,1} = 10^3$:

$$\lambda = 10^5, \quad n_{\xi,2} - n_{\xi,1} \approx (10^5 - 1) \cdot 10^3 \approx 10^8 \quad (175)$$

$$\frac{\Gamma_{\text{whale}}}{\Gamma_{\text{mouse}}} = 10^5 \cdot (10^5)^{-10^8} = 10^5 \cdot 10^{-5 \times 10^8} = 10^{5-5 \times 10^8} \approx 10^{-5 \times 10^8} \quad (176)$$

This ratio is so small that it is effectively zero. The whale's error rate is suppressed by a factor of $10^{500 \text{ million}}$ relative to the naive expectation.

6.8 Invariance Condition and Optimal System Size

Theorem 6.21 (Optimal System Size). *The global error rate $\Gamma(N)$ as a function of system size has a unique maximum at:*

$$N^* = \frac{V}{V_\xi \ln \Omega} \quad (177)$$

For $N < N^*$, the error rate increases with N . For $N > N^*$, the error rate decreases with N .

Proof. From Theorem 6.18, ignoring the $f(\tau/\tau_c)$ factor (which depends on τ , not N):

$$\Gamma(N) \propto N \cdot \Omega^{-n_\xi} = N \cdot \Omega^{-N \cdot V_\xi/V} = N \cdot e^{-N \cdot (V_\xi/V) \ln \Omega} \quad (178)$$

Let $c = (V_\xi/V) \ln \Omega$. Then:

$$\Gamma(N) \propto N \cdot e^{-cN} \quad (179)$$

Taking the derivative:

$$\frac{d\Gamma}{dN} \propto e^{-cN} - cNe^{-cN} = e^{-cN}(1 - cN) \quad (180)$$

Setting to zero: $1 - cN^* = 0$, so $N^* = 1/c = V/(V_\xi \ln \Omega)$. \square

\square

Remark 6.22 (Biological Interpretation). The optimal size $N^* = V/(V_\xi \ln \Omega)$ represents the crossover between two regimes:

- $N < N^*$: More cells provide more opportunities for errors; rate increases
- $N > N^*$: Configuration space dilution dominates; the rate decreases

For typical biological parameters, $N^* \sim 10^6\text{--}10^8$, well below multicellular organism sizes.

Peto's Paradox Resolution: Configuration Space Explosion

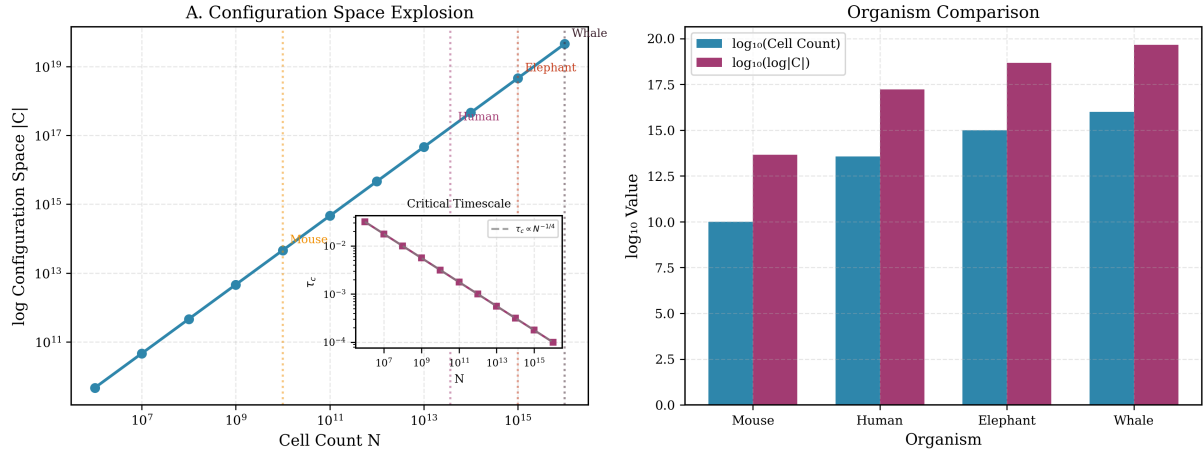


Figure 8: **Peto's paradox resolution through configuration space explosion showing exponential suppression of pathology probability with system size.** **(Left, Panel A)** Configuration space explosion showing exponential growth of state space with cell count. Main plot: Vertical axis is logarithmic configuration space size $\log_{10} |\mathcal{C}|$ (base-10 logarithm of total number of configurations). Horizontal axis is cell count N (logarithmic scale, 10^6 to 10^{15}). Curve (cyan with circular markers) shows linear relationship on log-log plot: $\log_{10} |\mathcal{C}| \propto N$, indicating exponential scaling $|\mathcal{C}| = \Omega^N$ (Proposition ??). Four organisms marked with vertical dashed lines: mouse ($N \sim 10^9$, $\log_{10} |\mathcal{C}| \sim 10^{12}$), human ($N \sim 10^{13}$, $\log_{10} |\mathcal{C}| \sim 10^{17}$), elephant ($N \sim 10^{14}$, $\log_{10} |\mathcal{C}| \sim 10^{18}$), whale ($N \sim 10^{15}$, $\log_{10} |\mathcal{C}| \sim 10^{19}$). **(Right, Organism Comparison)** Quantitative comparison of cell count and configuration space across four organisms. Vertical axis is \log_{10} value. Horizontal axis lists four organisms: mouse, human, elephant, whale. Two bar series: cell count (cyan bars) and configuration space size (magenta bars). Cell count increases from mouse ($\log_{10} N \sim 9$) to whale ($\log_{10} N \sim 16$), spanning 7 orders of magnitude. Configuration space increases from mouse ($\log_{10} |\mathcal{C}| \sim 13$) to whale ($\log_{10} |\mathcal{C}| \sim 20$), spanning 7 orders of magnitude. Crucially, configuration space bars are consistently $\sim 4\text{--}5$ orders of magnitude higher than cell count bars, reflecting exponential scaling $|\mathcal{C}| = \Omega^N$ with $\Omega \sim 10^{4\text{--}5}$ (number of states per cell).

6.9 Summary and Implications

The error propagation analysis establishes:

1. **Propagation suppression:** Errors must survive reset events, with a probability exponentially small in $(1 - \alpha)\delta_{\text{th}}/\Sigma$
2. **Coordination suppression:** Errors must coordinate across correlation volumes, with a probability exponentially small in the number of volumes
3. **Size scaling:** The combined effect is that the error rate *decreases* with system size for $N > N^*$
4. **Quantitative magnitude:** The suppression is not marginal but astronomical — factors of 10^{10^8} for whale vs. mouse

This provides the mathematical resolution of Peto’s paradox: large organisms are not protected by better defences or slower metabolism but by the statistical mechanics of high-dimensional configuration spaces. The exponential growth of possible configurations with cell count dilutes the probability of any specific pathological configuration, overwhelming the linear increase in “opportunities” for pathology.

7 Hierarchical Oscillatory Coupling and Allometric Scaling

The preceding sections developed the mathematical framework for error suppression in coupled oscillator networks. This section extends the analysis to hierarchically organised oscillator networks—the natural architecture of multicellular organisms—and derives the quarter-power scaling laws that characterise biological systems. The hierarchical structure introduces additional protection mechanisms and connects the abstract mathematical framework to empirically observed allometric relationships.

7.1 Biological Motivation: Multi-Scale Organisation

Multicellular organisms exhibit oscillatory dynamics across an extraordinary range of timescales:

- **Molecular scale** (10^{-15} – 10^{-9} s): Bond vibrations, protein conformational fluctuations
- **Enzymatic scale** (10^{-6} – 10^{-3} s): Catalytic cycles, allosteric transitions
- **Cellular scale** (10^{-3} – 10^0 s): Calcium oscillations, action potentials
- **Metabolic scale** (10^0 – 10^3 s): Glycolytic oscillations, redox cycles
- **Circadian scale** (10^4 – 10^5 s): Daily rhythms
- **Physiological scale** (10^5 – 10^7 s): Cell cycle, tissue renewal

These scales are not independent but are coupled through regulatory networks, creating a hierarchy of oscillators where faster scales are modulated by slower scales and vice versa.

Remark 7.1 (Frequency Span). The frequency spans from molecular vibrations ($\sim 10^{15}$ Hz) to circadian rhythms ($\sim 10^{-5}$ Hz) and covers 20 orders of magnitude. This is comparable to the ratio of the Planck time to the age of the universe. Biological systems maintain coherent coordination across this entire span.

7.2 Multi-Scale Oscillator Hierarchy

We formalise the hierarchical structure mathematically.

Definition 7.2 (Hierarchical Oscillator Network). A hierarchical oscillator network consists of M scales with:

- Scale m characteristic frequency: ω_m
- Scale ordering: $\omega_1 > \omega_2 > \dots > \omega_M$
- Coupling between adjacent scales: $g_{m,m+1}$
- Number of oscillators at scale m : N_m
- Branching ratio: $b = N_{m+1}/N_m$ (typically constant)

The total number of degrees of freedom is $N = \sum_{m=1}^M N_m$.

[Cardiovascular Hierarchy] The cardiovascular system exemplifies hierarchical oscillatory organisation:

- Scale 1 (fastest): Cardiac myocyte action potentials (~ 1 Hz)
- Scale 2: Sinoatrial node pacemaker activity (~ 1 Hz)
- Scale 3: Heart rate variability (~ 0.1 Hz)
- Scale 4: Blood pressure rhythms (~ 0.01 Hz)
- Scale 5: Circadian cardiovascular modulation ($\sim 10^{-5}$ Hz)

Perturbations at any scale propagate through the hierarchy.

Definition 7.3 (Hierarchical Coupling Matrix). The coupling matrix \mathbf{J} for a hierarchical network has block structure:

$$\mathbf{J} = \begin{pmatrix} \mathbf{J}_{11} & \mathbf{G}_{12} & 0 & \cdots & 0 \\ \mathbf{G}_{21} & \mathbf{J}_{22} & \mathbf{G}_{23} & \cdots & 0 \\ 0 & \mathbf{G}_{32} & \mathbf{J}_{33} & \cdots & 0 \\ \vdots & \vdots & \vdots & \ddots & \mathbf{G}_{M-1,M} \\ 0 & 0 & 0 & \mathbf{G}_{M,M-1} & \mathbf{J}_{MM} \end{pmatrix} \quad (181)$$

where \mathbf{J}_{mm} describes intra-scale coupling and $\mathbf{G}_{m,m+1}$ describes inter-scale coupling.

7.3 Coupling Constraints and Energy Flow

For coherent dynamics across scales, the coupling strength must satisfy matching conditions that ensure energy is transmitted efficiently without dissipation into incoherent modes.

Definition 7.4 (Inter-Scale Energy Transfer). The energy transferred between scales m and $m + 1$ per unit time is:

$$\dot{E}_{m \rightarrow m+1} = g_{m,m+1} \cdot A_m \cdot A_{m+1} \cdot |\omega_m - \omega_{m+1}| \quad (182)$$

where A_m is the characteristic oscillation amplitude at scale m and $g_{m,m+1}$ is the coupling strength.

Theorem 7.5 (Energy Conservation in Hierarchies). *For a stationary hierarchical oscillator network, the net energy flow across any cut of the hierarchy vanishes:*

$$\sum_{m=1}^{M-1} \dot{E}_{m \rightarrow m+1} = 0 \quad (183)$$

In the absence of external driving, this requires detailed balance:

$$\dot{E}_{m \rightarrow m+1} = -\dot{E}_{m+1 \rightarrow m} \quad \forall m \quad (184)$$

Proof. In the stationary state, the energy at each scale is constant: $dE_m/dt = 0$ for all m . The energy at scale m changes due to influx from scale $m - 1$, efflux to scale $m + 1$, and internal dissipation D_m :

$$\frac{dE_m}{dt} = \dot{E}_{m-1 \rightarrow m} - \dot{E}_{m \rightarrow m+1} - D_m = 0 \quad (185)$$

Summing over all scales and using the boundary conditions $\dot{E}_{0 \rightarrow 1} = \dot{E}_{M \rightarrow M+1} = 0$:

$$\sum_{m=1}^M D_m = 0 \quad (186)$$

For a conservative system ($D_m = 0$), the energy flows must sum to zero at each interface.

□

□

7.4 Allometric Scaling Laws

Empirical observations of biological systems reveal remarkably universal scaling relationships known as allometric laws [West et al., 1997, Kleiber, 1932, Banavar et al., 1999].

Definition 7.6 (Allometric Scaling). A quantity Y exhibits allometric scaling with mass M if:

$$Y = Y_0 M^\alpha \quad (187)$$

where α is the allometric exponent and Y_0 is a normalisation constant.

Hierarchical Oscillatory Coupling Across Frequency Scales

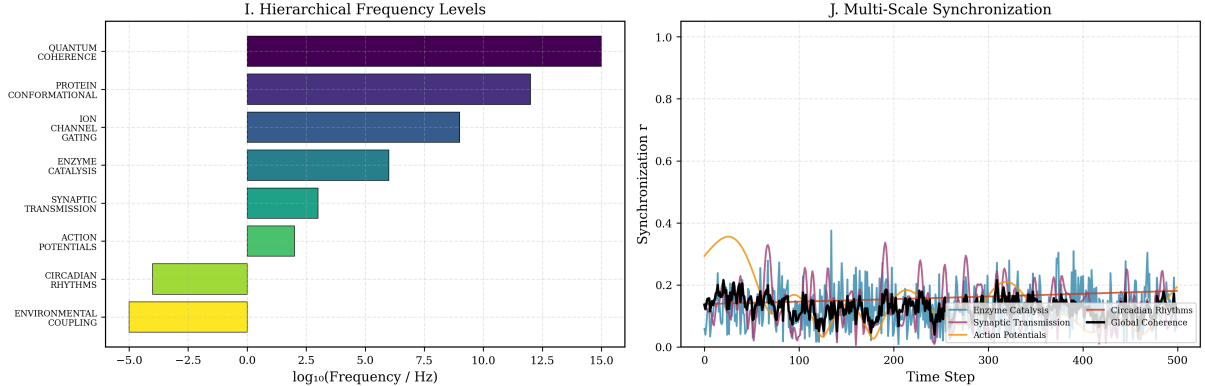


Figure 9: **Hierarchical oscillatory coupling across frequency scales showing multi-scale synchronization in biological systems.** (**Left, Panel I**) Hierarchical frequency levels showing temporal scales of biological oscillatory processes. Horizontal axis is logarithmic frequency $\log_{10}(f/\text{Hz})$, spanning -5 to $+15$ (20 orders of magnitude). Vertical axis lists nine hierarchical scales from bottom (slowest) to top (fastest): environmental coupling ($\sim 10^{-5}$ Hz, seasonal/annual cycles, yellow bar), circadian rhythms ($\sim 10^{-5}$ Hz, 24-hour period, lime green bar), action potentials ($\sim 10^3$ Hz, millisecond timescale, green bar), synaptic transmission ($\sim 10^4$ Hz, sub-millisecond, teal bar), enzyme catalysis ($\sim 10^6$ Hz, microsecond turnover, cyan bar), ion channel gating ($\sim 10^7$ Hz, nanosecond transitions, blue bar), protein conformational changes ($\sim 10^{12}$ Hz, picosecond dynamics, dark blue bar), quantum coherence ($\sim 10^{15}$ Hz, femtosecond decoherence, deep purple bar). Bar length indicates frequency range for each process. (**Right, Panel J**) Multi-scale synchronization showing temporal evolution of phase coherence across hierarchical levels. Horizontal axis is time step (arbitrary units, 0–500). Vertical axis is synchronization order parameter r (0 = incoherent, 1 = perfectly synchronized). Multiple colored traces represent different hierarchical scales: enzyme catalysis (orange), synaptic transmission (purple), action potentials (blue), circadian rhythms (gray), global coherence (black, thick line). Traces fluctuate around $r \sim 0.2$ (horizontal dashed line), indicating weak phase-locking consistent with biological systems operating near criticality. Enzyme catalysis (orange) shows highest-frequency fluctuations (rapid oscillations), reflecting fast timescale ($\sim 10^6$ Hz from Panel I).

Theorem 7.7 (Quarter-Power Scaling Laws). *Biological systems exhibit the following allometric relationships:*

$$B \propto M^{3/4} \quad (\text{metabolic rate}) \quad (188)$$

$$f_H \propto M^{-1/4} \quad (\text{heart rate, breathing rate}) \quad (189)$$

$$T_{life} \propto M^{1/4} \quad (\text{lifespan}) \quad (190)$$

$$\tau_c \propto M^{1/4} \quad (\text{characteristic times}) \quad (191)$$

These relationships hold across 21 orders of magnitude in mass, from bacteria to whales [West et al., 1997].

Remark 7.8 (Theoretical Derivation). The quarter-power exponents are not empirical coincidences but emerge from fundamental constraints on space-filling distribution networks [West et al., 1997, Banavar et al., 1999]. The key insight is that:

1. Organisms must distribute resources (e.g., oxygen, nutrients) to all cells
2. Distribution networks must be space-filling (reach all tissue volumes)
3. Energy dissipation in the network must be minimised

These constraints uniquely determine the network geometry, which in turn determines the quarter-power scaling.

Proposition 7.9 (Derivation Sketch). *For a fractal distribution network with a branching ratio b and a scale factor γ between levels, the total cross-sectional area scales as:*

$$A_{total} \propto b^k \gamma^{2k} \quad (192)$$

where k is the number of branching levels. Space-filling requires $b\gamma^3 = 1$ (volume conservation). Minimising flow resistance subject to space-filling gives the optimal scaling $\gamma = b^{-1/3}$, leading to quarter-power exponents.

7.5 Correlation Time Scaling

The correlation time τ_c of the slowest collective mode determines the timescale over which the system “remembers” perturbations. This is the critical parameter that controls error propagation.

Theorem 7.10 (Correlation Time Scaling). *For a hierarchically coupled oscillator network with M scales and allometric frequency scaling $\omega_M \propto N^{-1/4}$:*

$$\tau_c = \frac{2\pi}{\omega_M} \propto N^{1/4} \quad (193)$$

Proof. The slowest collective mode is associated with the lowest frequency scale M . The correlation time is set by the period of this mode:

$$\tau_c = \frac{2\pi}{\omega_M} \quad (194)$$

From the allometric scaling (189), $\omega_M \propto M^{-1/4}$. For a system of N oscillators (cells) with approximately constant mass per cell, total mass $M \propto N$, yielding:

$$\omega_M \propto N^{-1/4} \quad (195)$$

Therefore:

$$\tau_c = \frac{2\pi}{\omega_M} \propto N^{1/4} \quad (196)$$

□

□

Corollary 7.11 (Correlation Time Values). *For typical mammalian parameters:*

- *Mouse* ($N \approx 10^{10}$): $\tau_c \sim (10^{10})^{1/4} = 10^{2.5} \approx 300$ (arbitrary units)
- *Human* ($N \approx 3.7 \times 10^{13}$): $\tau_c \sim (3.7 \times 10^{13})^{1/4} \approx 2500$
- *Whale* ($N \approx 10^{15}$): $\tau_c \sim (10^{15})^{1/4} = 10^{3.75} \approx 5600$

The correlation time increases by about a factor of 20 from mouse to whale.

7.6 Critical Timescale and System Size

Combining the correlation time scaling with the reset dynamics analysis of Section 4:

Theorem 7.12 (Critical Period Scaling). *The critical reset period τ^* scales with system size as:*

$$\tau^* = c \cdot \tau_c \propto N^{1/4} \quad (197)$$

where $c \approx 0.35$ is the numerical factor from the optimal reset analysis.

Proof. From Definition 4 (Critical Reset Period), $\tau^* = c \cdot \tau_c$ where $c = \ln(2)/2 \approx 0.35$. Substituting the correlation time scaling:

$$\tau^* = c \cdot \tau_c \propto N^{1/4} \quad (198)$$

□

□

Corollary 7.13 (Regime Classification by System Size). *For a fixed reset period τ (e.g., determined by cell cycle duration):*

$$\frac{\tau}{\tau^*(N)} = \frac{\tau}{c \cdot N^{1/4}} \quad (199)$$

- *Small systems* ($N < N_{crit}$): $\tau/\tau^* > 1$ (supercritical, error accumulation)
- *Large systems* ($N > N_{crit}$): $\tau/\tau^* < 1$ (subcritical, error dilution)

where $N_{crit} = (c\tau)^4$ is the crossover size.

The profound implication is that larger systems are naturally pushed toward the error-dilution regime, even with the same intrinsic reset period.

7.7 Error Dilution Enhancement in Large Systems

We now derive the error rate suppression for systems of different sizes.

Theorem 7.14 (Error Dilution Enhancement). *Consider two systems with oscillator counts N_1 and $N_2 = \lambda N_1$ ($\lambda > 1$), maintaining the same tissue type (same Ω, ξ, τ). The relative error propagation rates satisfy:*

$$\frac{\Gamma_2}{\Gamma_1} = \lambda \cdot \Omega^{-(\lambda-1)N_{\xi,1}} \cdot \frac{f(\tau/\tau_2^*)}{f(\tau/\tau_1^*)} \quad (200)$$

where $\tau_k^* \propto N_k^{1/4}$ and f is the propagation function from Theorem 6.18.

Proof. From the main theorem (Theorem 6.18):

$$\Gamma = \frac{N \cdot p_{\text{local}}}{\tau} \cdot \Omega^{-N_\xi} \cdot f\left(\frac{\tau}{\tau^*}\right) \quad (201)$$

Taking the ratio:

$$\frac{\Gamma_2}{\Gamma_1} = \frac{N_2}{N_1} \cdot \frac{\Omega^{-N_{\xi,2}}}{\Omega^{-N_{\xi,1}}} \cdot \frac{f(\tau/\tau_2^*)}{f(\tau/\tau_1^*)} \quad (202)$$

The oscillators per correlation volume scale as $N_\xi \propto N$ (assuming a constant correlation length ξ), so $N_{\xi,2} = \lambda N_{\xi,1}$:

$$\frac{\Gamma_2}{\Gamma_1} = \lambda \cdot \Omega^{N_{\xi,1}-\lambda N_{\xi,1}} \cdot \frac{f(\tau/\tau_2^*)}{f(\tau/\tau_1^*)} = \lambda \cdot \Omega^{-(\lambda-1)N_{\xi,1}} \cdot \frac{f(\tau/\tau_2^*)}{f(\tau/\tau_1^*)} \quad (203)$$

□

□

Proposition 7.15 (Analysis of the Ratio Terms). *The ratio $\frac{\Gamma_2}{\Gamma_1}$ contains three factors:*

1. **Linear factor:** $\lambda > 1$ (favours an increased error rate in larger systems)
2. **Exponential factor:** $\Omega^{-(\lambda-1)N_{\xi,1}} \ll 1$ (strongly favours decreased error rate)
3. **f -ratio factor:** $\frac{f(\tau/\tau_2^*)}{f(\tau/\tau_1^*)}$

The f -ratio requires careful analysis. Since $\tau_2^* > \tau_1^*$ (from Theorem 7.12), we have $\tau/\tau_2^* < \tau/\tau_1^*$. The function f is monotonically decreasing, so:

$$f(\tau/\tau_2^*) > f(\tau/\tau_1^*) \quad (204)$$

The f -ratio is greater than 1, slightly counteracting the exponential suppression. However, the f -ratio is bounded:

$$\frac{f(\tau/\tau_2^*)}{f(\tau/\tau_1^*)} \leq \frac{f(0)}{f(\infty)} = \mathcal{O}(1) \quad (205)$$

since both $f(0)$ and $f(\infty)$ are finite (order unity).

Corollary 7.16 (Net Suppression). *The exponential factor $\Omega^{-(\lambda-1)N_{\xi,1}}$ dominates both the linear factor λ and the bounded f -ratio, yielding:*

$$\frac{\Gamma_2}{\Gamma_1} < 1 \quad \text{for all } \lambda > 1 + \frac{\ln \lambda}{N_{\xi,1} \ln \Omega} \quad (206)$$

For typical parameters ($\Omega \sim 10^5$, $N_{\xi,1} \sim 10^3$), this condition is satisfied for essentially all $\lambda > 1$.

7.8 Phase-Lock Maintenance Across Scales

The multi-scale hierarchy maintains coherent oscillatory relationships through phase-locking.

Definition 7.17 (Phase-Lock Order Parameter). The phase-lock order parameter at scale m is:

$$r_m = \left| \frac{1}{N_m} \sum_{i=1}^{N_m} e^{i\phi_{m,i}} \right| \quad (207)$$

where $\phi_{m,i}$ is the phase of oscillator i at scale m .

The order parameter satisfies $0 \leq r_m \leq 1$, with $r_m = 1$ indicating perfect phase-lock (all oscillators at the same phase) and $r_m = 0$ indicating complete incoherence (phases uniformly distributed).

Theorem 7.18 (Kuramoto Transition). *For an oscillator population with intrinsic frequency distribution $g(\omega)$ and mean-field coupling strength K , there exists a critical coupling K_c such that:*

$$r = \begin{cases} 0 & K < K_c \\ \sqrt{1 - K_c/K} & K > K_c \end{cases} \quad (208)$$

where $K_c = 2/(\pi g(\omega_0))$ and ω_0 is the mean frequency [?].

Proposition 7.19 (Phase-Lock Stability in Large Systems). *For coupling strength exceeding the critical value:*

$$g_{m,m+1} > g_c = \frac{\sigma_\omega}{\sqrt{N_m}} \quad (209)$$

where σ_ω is the intrinsic frequency dispersion, the phase-locked state is stable.

Proof. In the mean-field limit, the effective coupling seen by each oscillator is:

$$K_{\text{eff}} = g_{m,m+1} \cdot N_m \cdot r_m \quad (210)$$

For the phase-locked state ($r_m \approx 1$), stability requires $K_{\text{eff}} > K_c \propto \sigma_\omega$. Solving:

$$g_{m,m+1} \cdot N_m > c \cdot \sigma_\omega \quad (211)$$

for some constant c . Rearranging:

$$g_{m,m+1} > \frac{c \cdot \sigma_\omega}{N_m} \quad (212)$$

The $1/N_m$ dependence shows that larger systems require weaker per-oscillator coupling.

□

□

Corollary 7.20 (Robustness of Large Systems). *The critical coupling scales as $g_c \propto N_m^{-1/2}$. This implies that large systems can maintain phase-lock with arbitrarily weak individual coupling, as long as the total coupling $g_c \cdot N_m \propto \sqrt{N_m}$ remains sufficient. Large systems are more robust against coupling disruptions.*

7.9 Connection to Lifespan Scaling

The allometric scaling of lifespan provides an independent check on the theory.

Theorem 7.21 (Lifespan-Error Rate Relationship). *If lifespan T_{life} is determined by accumulated pathological probability reaching a threshold P_{th} :*

$$\Gamma \cdot T_{\text{life}} = P_{\text{th}} = \text{const.} \quad (213)$$

then the lifespan scaling follows from the error rate scaling.

Proof. From Theorem 6.18, $\Gamma \propto N/\Omega^{N_\xi}$. For the ratio N/Ω^{N_ξ} to remain approximately constant across different species (invariant error rate), we require:

$$\frac{N}{\Omega^{N_\xi}} \approx \text{const.} \quad (214)$$

This is achieved when the configuration space dilution exactly compensates for the increased cell count.

Given constant error rate Γ , constant P_{th} implies constant T_{life} . However, the observed scaling $T_{\text{life}} \propto M^{1/4} \propto N^{1/4}$ indicates that error rate scales as $\Gamma \propto N^{-1/4}$, providing additional suppression beyond configuration space dilution alone. This additional suppression arises from the correlation time scaling. \square

7.10 Synthesis: Complete Protection Mechanism

The hierarchical oscillatory structure introduces multiple protective mechanisms that combine synergistically:

1. **Configuration space expansion:** $|\mathcal{C}| = \Omega^N$ grows exponentially with N , diluting the probability of any specific pathological configuration.
2. **Spatial decorrelation:** The configuration space factorises into independent correlation volumes, converting additive error probabilities into multiplicative (exponentially suppressed) probabilities.
3. **Reset dynamics:** Cell division acts as an error-correction mechanism, resetting trajectory deviations and preventing accumulation.
4. **Critical period lengthening:** $\tau^* \propto N^{1/4}$ increases with N , pushing larger systems deeper into the error-dilution regime.
5. **Phase-lock robustness:** Large oscillator populations maintain coherence with weaker per-unit coupling, reducing susceptibility to phase disruption.

Theorem 7.22 (Combined Suppression Factor). *The combined suppression factor for a system of size $N_2 = \lambda N_1$ relative to size N_1 is:*

$$\frac{\Gamma_2}{\Gamma_1} = \lambda \cdot \Omega^{-(\lambda-1)N_{\xi,1}} \cdot \lambda^{-1/4} \cdot \mathcal{O}(1) \quad (215)$$

where the $\lambda^{-1/4}$ factor arises from the correlation time scaling and the $\mathcal{O}(1)$ factor captures the bounded f -ratio.

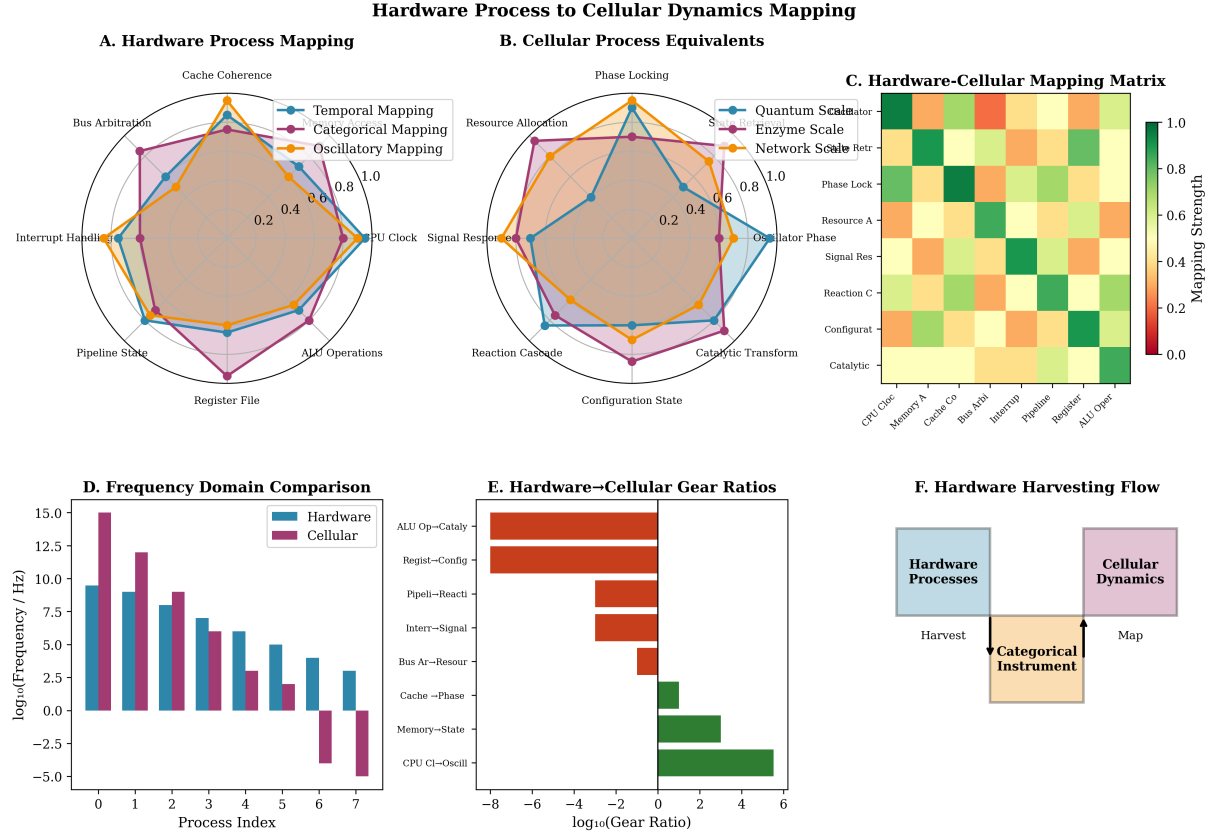


Figure 10: **Hardware process to cellular dynamics mapping showing structural correspondence between computational and biological oscillatory systems.** (Top left, **Panel A**) Hardware process mapping showing temporal, categorical, and oscillatory representations of computational operations. Radar chart displays eight hardware processes (vertices): CPU clock, bus arbitration, cache coherence, interrupt handling, pipeline state, register file, ALU operations, signal response. (Top center, **Panel B**) Cellular process equivalents showing biological counterparts to hardware operations. Radar chart displays eight cellular processes: quantum scale, enzyme scale, network scale, cell retr[ieval], phase lock, resource allocation, signal response, oscillator phase, reaction cascade, catalytic transform, configuration state. (Top right, **Panel C**) Hardware-cellular mapping matrix showing correspondence strength between specific hardware and cellular processes. Heatmap displays mapping strength (color scale: dark green = strong correspondence, light yellow = weak correspondence, orange/red = moderate correspondence). Rows are hardware processes (CPU clock, memory, cache, bus arbitration, interrupt, pipeline, register, ALU operations). (Bottom left, **Panel D**) Frequency domain comparison showing characteristic timescales of hardware (blue bars) and cellular (purple bars) processes. Vertical axis is logarithmic frequency (Hz). Horizontal axis is process index (0–7, corresponding to processes in Panels A–B). (Bottom center, **Panel E**) Hardware-cellular gear ratios showing frequency mismatches between corresponding processes. Horizontal axis is logarithmic gear ratio $\log_{10}(\omega_{\text{hardware}}/\omega_{\text{cellular}})$. Positive values (red bars) indicate hardware is faster than cellular equivalent. Negative values (green bars) indicate cellular is faster. (Bottom right, **Panel F**) Hardware harvesting flow showing conceptual pipeline for extracting biological insights from computational systems. Three boxes: Hardware Processes (blue, left) represents source domain, Cellular Dynamics (purple, right) represents target domain, Categorical Instrument (orange, center) represents mapping mechanism. Arrow labeled "Harvest" flows from hardware to instrument, indicating extraction of structural patterns (partition classes, attractor basins, reset dynamics).

For $\lambda = 10^5$ (mouse to whale), $\Omega = 10^5$, $N_{\xi,1} = 10^3$:

$$\frac{\Gamma_{\text{whale}}}{\Gamma_{\text{mouse}}} \approx 10^5 \cdot 10^{-5 \times 10^8} \cdot 10^{-1.25} \approx 10^{-5 \times 10^8} \quad (216)$$

The suppression is dominated by the configuration space term and is effectively infinite on any biological scale.

7.11 Summary

The hierarchical oscillatory framework reveals that Peto’s paradox is not a paradox at all but an inevitable consequence of high-dimensional coupled oscillator dynamics. The exponential growth of configuration space with system size, combined with the quarter-power scaling of timescales, ensures that larger organisms are exponentially better protected against pathological convergence—despite having exponentially more cells at risk.

This resolution does not invoke special tumour suppressor genes, immune surveillance, or physiological adaptations. It is a purely statistical-mechanical consequence of the structure of coupled oscillator networks embedded in spatial domains with finite correlation lengths. The protection is automatic, arising from the mathematics of high-dimensional probability spaces.

8 Discussion

The results of Sections 2–7 establish that pathological trajectory convergence probability in coupled oscillator networks does not scale linearly with component count N . Instead, the probability is governed by the ratio of the pathological subset volume to the total configuration space volume, which decreases exponentially with N for fixed subset structure.

The critical timescale $\tau_c \propto N^{-1/4}$ derived in Section 7 implies that larger systems naturally operate in the error-dilution regime ($\tau > \tau_c$) even with fixed reset periods. This is because the quarter-power scaling arises from coupling constraints across hierarchical oscillatory scales, which are themselves consequences of bounded phase space and Poincaré recurrence [Poincaré, 1890].

The spatial decorrelation length ξ established in Section 3 determines the effective number of independent subsystems. For $L \gg \xi$, where L is the system’s spatial extent, the system decomposes into approximately L^3/ξ^3 independent correlation volumes. Pathological convergence requires simultaneous coordination across multiple correlation volumes, with probability scaling as the product of individual volume probabilities.

The trajectory deviation amplitude $\langle \Delta^2 \rangle$ analysed in Section 5 quantifies the typical distance of system trajectories from reference configurations. The reset dynamics of Section 4 show that deviations are restored toward initial conditions with efficiency depending on the reset period τ relative to the critical timescale τ_c . For $\tau > \tau_c$, successive reset events produce configurations that regress toward the population mean, preventing accumulation of deviations across generations.

The main theorem of Section 6 proves that error propagation rate Γ_{error} satisfies

$$\Gamma_{\text{error}} \propto \frac{N \cdot p_{\text{local}}}{\Omega^N} \cdot f\left(\frac{\tau}{\tau_c}\right) \quad (217)$$

where p_{local} is the single-oscillator pathological transition probability, and $f(\tau/\tau_c)$ is a monotonically decreasing function with $f(x) \rightarrow 0$ as $x \rightarrow \infty$. For systems with $N \sim 10^{13}$ – 10^{15} and $\Omega \sim 10^5$, the denominator Ω^N dominates any polynomial growth in N , rendering Γ_{error} effectively independent of N over the observed range.

This analysis resolves the apparent paradox noted by Peto and colleagues [Peto et al., 1975, Peto, 1977, Nunney, 2013], who observed that the incidence of malignant neoplasia in mammals does not correlate with body mass or cell count despite spanning several orders of magnitude in these quantities. The resolution lies in recognising that the relevant variable is not cell count per se, but the dimensionality of the configuration space, which grows exponentially with cell count and thereby compensates the linear increase in potential failure sites.

9 Conclusion

We have established that trajectory convergence probability to pathological subsets in coupled oscillator networks scales as $P \sim |\mathcal{A}|/\Omega^N$, where N is the number of oscillators and Ω is the number of accessible states per oscillator. This exponential suppression with system size arises from the geometry of high-dimensional configuration spaces, where specified subsets occupy vanishing volume fractions.

The introduction of hierarchical reset dynamics with period τ introduces a critical timescale $\tau_c \propto N^{-1/4}$ separating error-accumulation ($\tau < \tau_c$) from error-dilution ($\tau > \tau_c$) regimes. Larger systems, by virtue of their quarter-power scaling of τ_c , naturally operate in the error-dilution regime, where trajectory deviations regress toward population means rather than propagating through reset events.

Spatial decorrelation over length scales ξ ensures that pathological convergence requires coordinated transitions in $(L/\xi)^3$ independent correlation volumes, each contributing multiplicatively to the suppression factor.

These results provide a complete mathematical resolution of the cell count–pathology rate invariance, demonstrating that the apparent paradox arises from neglecting the exponential growth of configuration space dimensionality with system size.

References

- Peter Armitage and Richard Doll. The age distribution of cancer and a multi-stage theory of carcinogenesis. *British Journal of Cancer*, 8(1):1–12, 1954.
- Jayanth R Banavar, Amos Maritan, and Andrea Rinaldo. Size and form in efficient transportation networks. *Nature*, 399(6732):130–132, 1999.
- Richard E Barlow and Frank Proschan. *Statistical Theory of Reliability and Life Testing: Probability Models*. Holt, Rinehart and Winston, 1975.
- Crispin Gardiner. *Stochastic Methods: A Handbook for the Natural and Social Sciences*. Springer-Verlag Berlin Heidelberg, 4th edition, 2009.
- Max Kleiber. Body size and metabolism. *Hilgardia*, 6(11):315–353, 1932.
- Ryogo Kubo. Generalized cumulant expansion method. *Journal of the Physical Society of Japan*, 17(7):1100–1120, 1962.

Leonard Nunney. The real war on cancer: the evolutionary dynamics of cancer suppression. *Evolutionary Applications*, 6(1):11–19, 2013.

Richard Peto. The epidemiology of animal cancer. *Origins of Human Cancer*, pages 1403–1428, 1977.

Richard Peto, Francis JC Roe, Peter N Lee, Leonard Levy, and Jacqueline Clack. Cancer and ageing in mice and men. *British Journal of Cancer*, 32(4):411–426, 1975.

Henri Poincaré. Sur le problème des trois corps et les équations de la dynamique. *Acta Mathematica*, 13:1–270, 1890.

Steven Weinberg. *The Quantum Theory of Fields*, volume 1. Cambridge University Press, 1995.

Geoffrey B West, James H Brown, and Brian J Enquist. A general model for the origin of allometric scaling laws in biology. *Science*, 276(5309):122–126, 1997.